Reconstructing environmental variability at Leynavatn, Faroe Islands

Master thesis in Quaternary Geology and Palaeoclimatology

Melissa M. Langnæs

Department of Earth Science

University of Bergen

June 2019

Abstract: A new continuous environmental reconstruction has been established based on a 390 cm long lake core from Leynavatn Streymoy (southeast Faroes Islands), containing sediments spanning from the last 550 CE (Common Era). To acquire further understanding, the lake core is compared to other proxy records from the North Atlantic region to examine the amplitude and timing of regional climate variability. A firm chronology is generated by radiocarbon dating from the sediments. In addition, magnetic susceptibility, loss-on-ignition, XRF-core scanning and X-ray CT-scanning were used to unravel different catchment activities. A simplified Quaternary geological map is proposed to explore the present activity and define different catchment processes.

Leynavatn sediment record suggest that the concentration of geochemical elements Ti, Ca and K, together with dry bulk density and magnetic susceptibility reflect changes in amount of inorganic delivery to the lake. In contrary, the geochemical ratio Incoh/Coh scattering and loss-on-ignition reflect variations in the organic input. These proxies are associated to landscape changes, which are sensitive to late Holocene climate variability and the human expansion at the Faroes.

The results from Leynavatn sediments indicate that all climatic induced phenomena including precipitation, atmosphere and sea surface temperatures, underwent an evident change at the transition from Medieval Warm Period to the Little Ice Age. The geochemical and geophysical changes in the lake sediments are associated with enhanced weathering and increased erosion around 1200-1400 CE, referring to the Medieval Warm Period. After 1400 CE a prolonged decrease in inorganic delivery propose a climatic cooling, where increasing frequency of cold summers and cold winters reflect the onset of the Little Ice Age.

Acknowledgement First, I would like to thank my supervisors Jostein Bakke and Eivind Støren for giving constructive comments, technical assistance, guidance and support. Also, a special thanks to Lis Mortensen, Jordan Doll Holl, Willem van der Bilt, Kenneth Mangersnes and Johannes Hardeng for their invaluable support, help in the coring procedures and assisting in the production of figures, models and maps in Bacon and ArcGIS.

I would also like to thank the master students at the Department of Earth Sciences for the great social environment the last five years. Especially, thanks to the students taking the course GEOV225 (spring 2018) for their assistance in the field. A special thanks to Ane Brun Bjerkås, Monika Øksnes, Eli Anne Støfring, Thale Damm-Johnsen and Anders Foss for helping me the past year and improving the manuscript.

Finally, I would like to thank my family and friends for emotional support and for carefully reading a draft of the study and giving helpful feedback.

Contents

1 Introduction

1.1 Objective

The objective of this study is to collect climate and environmental information from the Faroe Islands. The Holocene period is characterized with major changes, both in long-term and short-term climate signals (Andresen, Björck, Rundgren, Conley, & Jessen, 2006; Dugmore et al., 2005). In order to develop further understanding, the study is based on a multi-proxy record which extends from 550 CE to 2015 CE and considers current knowledge from numerous paleo studies. Specifically, an interval (1250-1375 CE) in the sediment record is investigated, because it shows a profound change in the radiocarbon dates, sediment accumulation rate and physical properties in the lake sediments. The study aims to answer these following questions:

- Combine geomorphological mapping of the area with lake sediment analysis to reconstruct and understand how the natural climate variability has affected the sediment accumulation in lake Leynavatn.
  - Identify landforms and Earth surface processes around Leynavatn and present an Quaternary geological map of the catchment area and the surrounding lake basin.
  - Use lake sediment properties to record potentially past climate over the late Holocene Epoch. Is there any evidence for anthropogenic influence in the lake record?

1.2 The use of lake sediments to reconstruct climate

The debate about the consequence of global climate change has shown interest in understanding past climate and the effect on Earth surface processes (Andresen et al., 2006). Therefore, past climate records such as historical documents, tree rings, ice cores, corals, speleothems, lake and marine sediments are important natural archives for understanding

and gathering knowledge about climate conditions and ongoing changes (Bradley, 2014, p. 1-5).

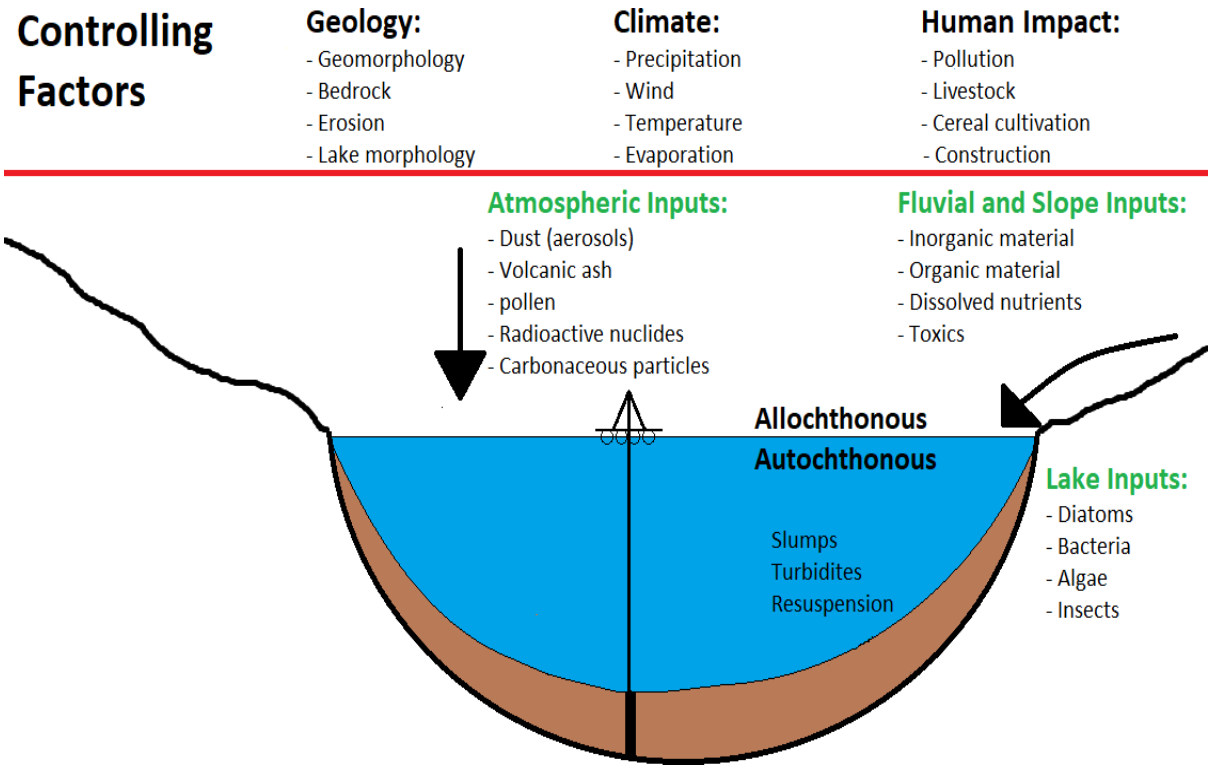

Figure 1: *Model illustrating potential Earth surface processes influencing the allochthonous and autochthonous material influx to the lake basin. Modified from (Bradley, 2014, p. 320).*

Lakes accumulate sediments from their surrounding environment and so sediment processes can be utilized as a key source of information, because the continuous lake sedimentation can be preserved for thousands of years (Bradley, 2014, p. 319-321) (Figure 1). Materials found in lake basins are made up of two components: allochthonous, originating from outside the lake basin, and autochthonous materials, produced within the lake. For instance, grain size and mineralogical composition can reveal the origin of allochthonous materials (T. Cronin, 2009, p. 2). Loess may be found in the lake sediments, giving some indirect information about wind activity and prevailing atmospheric circulation patterns. However, biological productivity in lakes may respond direct to climate change and their

fingerprints can reflect the water properties in the lake (Mcgowan, Grauert, & Anderson, 2008). Such climate archives (both allochthonous and autochthonous materials) can be useful in paleoclimatic reconstruction and can also show a response of disturbance connected with local geology, vegetation and relief in the catchment.

For a number of reasons, the Faroe Islands are an interesting area for geological studies. The archipelago has a key position in the context of geographical isolation, the absence of continental effects, short colonization period and the response to changes in atmospheric and oceanic temperature and circulation patterns. These factors may cause small regional climate fluctuation that can be recorded in lakes (Andresen et al., 2006; Kuijpers, Troelstra, Wisse, Heier Nielsen, & van Weering, 1998; Rasmussen & Thomsen, 2010). This study presents a well-dated, multi-proxy record from Streymoy to determine natural variability of late Holocene climate and environment. A combination of different techniques were used: physical (loss-on-ignition, magnetic susceptibility, x-ray fluorescence scanner and CT-scanner) and chronological (radiocarbon dating) analysis of 390 cm composite sediment core from a lake catchment system, Leynavatn.

2 Theoretical Background and Geological Framework

2.1 Study area

The Faroe Islands is a group of 18 islands situated in the North Atlantic region (latitude 62°N and longitude 7°W), approximately 675 km west from the Norwegian mainland, 300 km northwest of the Shetland Islands and 400 km east of Iceland (Andresen et al., 2006; Arge, Sveinbjarnardóttir, Edwards, & Buckland, 2005; Arge, 2014; Gathorne-Hardy et al., 2007; Jóhansen, 1985; Olsen et al., 2010) (Figure 2a). The islands have a total area of 1399 km^2 and extends 113 km from north to south and 75 km from east to west (Cappelen & Laursen, 1998). The Faroes is a small archipelago that consist of hilly islands of varying size, that are separated by narrow fjords and sounds (Gathorne-Hardy et al., 2007; Arge, 2014). It is also characterized by windswept, peatland and low-growing scrub vegetation. The islands rise steeply from the ocean to an altitude of 400-600 m a.s.l in the southern islands and 600-900 m a.s.l in the northern islands (Olsen et al., 2010; Humlum & Christiansen, 1998).

There are approximately 800 lakes and ponds, where numerous small lakes have potential to obtain paleoclimate information, both in decadal or centennial timescales (Mcgowan et al., 2008). The main location investigated in this study is lake Leynavatn (62°07′ N and 7°01′ W), situated southeast on the island Streymoy. The lake has previously been studied by Malmquist (2002), Landkildehus (2002) and McGowan (2008) and is c. 0.18 km^2, maximum length 680 m and width 350 m. The Maximum depth is measured to 33 m, while the average depth is 13.7 m (Malmquist, Ingimarsson, Jóhannsdóttir, Òlafsson, & Gíslason, 2002; Landkildehus, Jeppesen, Jensen, & Dali, 2002). Most lakes in the Faroes have relatively large catchments and Leynavatn catchment is around 16.6 km^2. Today, human interference in the catchment is a common occurrence. Especially the low-lying part of the Dalá valley consists of cultivated and extensive grass fields. There are several households and an old road along the lake shore. This road is replaced by a 760 m long tunnel called *Leynatunnilin* due to extensive degradation.

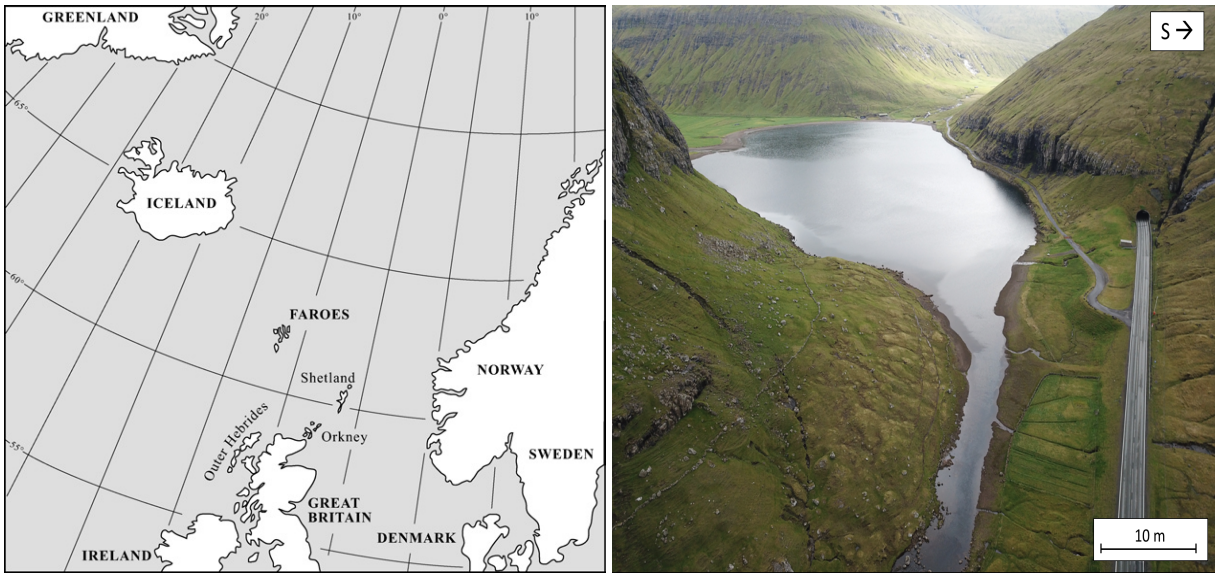

(a) (b)

Figure 2: *Overview of the study area. A) study site (Faroe Islands) location in the North Atlantic region (Arge et al., 2005; Edwards et al., 2005); B) Drone photograph of Leynavatn and the surrounding landscape. Notice, Leynatunnilin and the old road along the lake shore.*

2.2 Geological overview

2.2.1 Regional geology

The islands and its insular shelf constitute the basaltic Faroe platform, which outlines a triangular shape (Figure 3). The platform is bound to the east and southwest by two deep channels, the Faroe-Shetland Channel and the Faroe Bank Channel. These channels separates the Nordic seas from the Atlantic Ocean (Nielsen, Rasmussen, Ceramicola, & Kuijpers, 2007).

The Faroese archipelago is of volcanic origin and is part of the North Atlantic Igneous Province, which stretches from Ireland to Greenland. It is derived from erosional remnants of early Tertiary flood basalts (Nielsen et al., 2007; Olsen et al., 2010), that occurs when Greenland and Eurasia began drifting apart. The continental break-up was

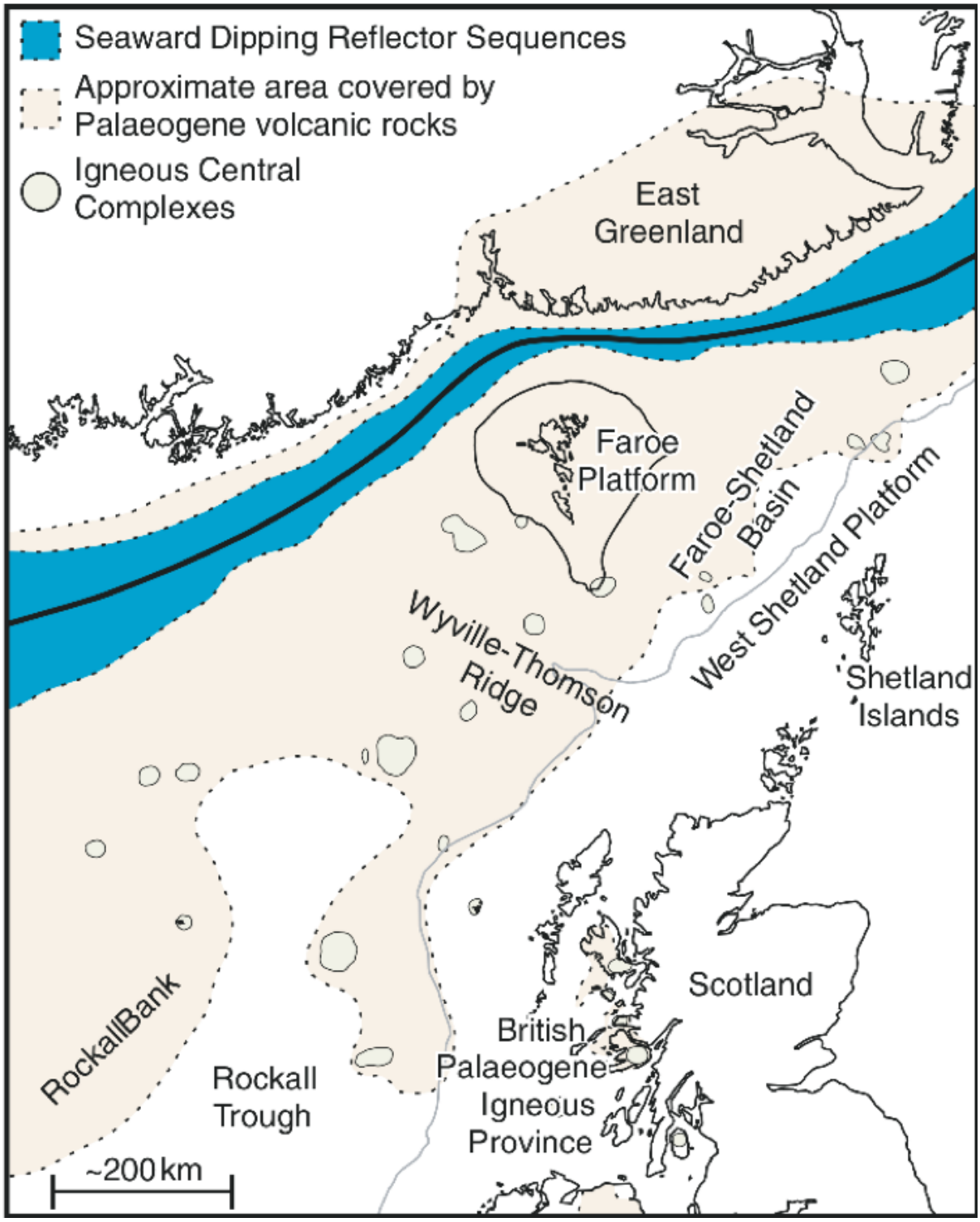

Figure 3: *Location of the Faroe platform, prior to the opening of the North Atlantic (Passey & Bell, 2007; Larsen et al., 1999).*

generated by the arrival of the proto-Iceland plume beneath Greenland during the Paleocene and early Eocene (62-54 Ma), resulting in widespread volcanic activity and the onset of seafloor spreading (Passey & Bell, 2007). Prior to the opening of the North Atlantic, the Faroe Platform and East Greenland were less than 120 km apart based on Larsen (1999) studies of plate reconstruction and geochemical correlation (Figure 3).

The Faroe Island Basalt Group (FIBG) has a great stratighraphic thickness of 6.6 km, divided into several formations based on lithologies and sills (Passey & Bell, 2007). Incorporated in the FIBG are intervening layers consisting of volcanic ashes, tuff, fluviatile conglomerates, clay and sandstone. In general, the layers tilt in an easterly direction (Guttesen, 1996).

2.2.2 Quaternary geology and glacial history

The topography of the islands show glacial imprints, where the erosion has formed features such as cirques, U-shape valleys, fjords and carved plateaus (Andresen et al., 2006; Humlum & Christiansen, 1998). During the last glaciation (Weichselian), the cold-climate accumulated several local ice caps (Humlum, Christiansen, Svensson, & Mortensen, 1996). Regional mapping of the glacier movement can be indicated by studying significant geological imprints, mostly erosional features reveal that striations radiate inn all directions from the larger islands. These features indicate that the ice caps covered the landscape up to 700 m a.s.l and extended beyond the present coastline (Humlum & Christiansen, 1998; Guttesen, 1996). Hence, very little is known about the Late Weichselian deglaciation and when the Faroes were Ice-free.

Previous investigations by Humlum (1998) has detected several moraine ridges, which has thought to be of Younger Dryas age (Wastegård, Björck, Grauert, & Hannon, 2001). He suggest that the archipelago were extensively covered by ice during parts of the Younger Dryas and that the initial deglaciation started at the end of this cold period. Compared to other heavily glaciated regions, there has not been found uplifted marine sediment on the islands. The absence of such deposits is interpreted as a consequence of a thin ice sheet in combination with an early deglaciation (Humlum, 1998)

2.3 Climate and environmental overview

2.3.1 Ocean currents around the Faroe Islands

The interaction between warm surface waters and cold deep waters is controlled by the enormous ocean conveyor belt system, termohaline circulation (THC). A number of processes contribute to the global THC flow pattern, which will be explained in further detail.

The ocean current system in the North Atlantic is complex. There are three main currents: The warm Norwegian Atlantic Current (NwAC), the cold East Greenland Current (EGC) and the East Icelandic Current (EIC) (Andersson, Risebrobakken, Jansen, & Dahl, 2003). The wind-driven movement of relatively warm and saline surface water masses to higher latitudes is associated with the North Atlantic Current (NAC). It is partly responsible for bringing northwest Europe, including the Faroese archipelago, heat and moisture (Andersson et al., 2003; Kuijpers et al., 1998). The NAC is advected into the Nordic seas, through the ridges between Iceland and Scotland shown in Figure 4. From there, it enters the shallow Barent sea and flows via the Fram strait into the Polar Ocean. In the arctic and polar regions air-sea interactions transforms the water masses to cool and dense water that contribute to the formation of the North Atlantic Deep Water (NADW) (Aken, 2007).

To compensate for the northward flowing water masses, the colder and less saline Arctic waters (e.g. Norwegian Sea overflow water) flow southwards, exporting deep water via two major gateways: the Denmark straits and the Faroe-Shetland Channel (Mcgowan et al., 2008). Water masses originating from the Arctic are volumetrically important components of NADW (Kuijpers et al., 1998). The EGC is one of the main sources of deep water in the northern hemisphere due to convective processes. It carries both surface and deeper water masses into the Iceland- and Norwegian Seas (Andersson et al., 2003). Thereafter, the southward export from the arctic will enter the deep North Atlantic Ocean and the Southern Ocean where they mix with the rest of the world‘s waters(Mcgowan et al., 2008).

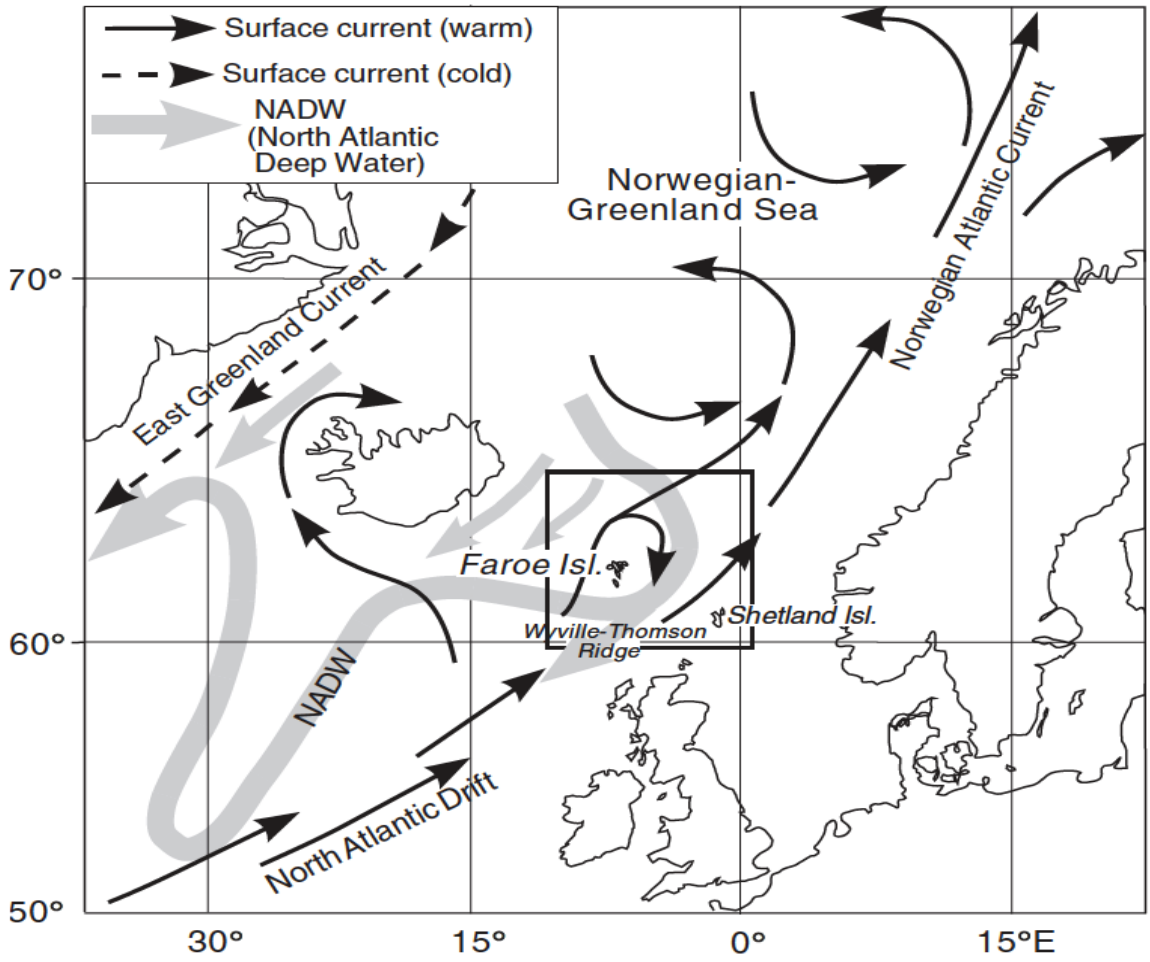

Figure 4: *Map of the ocean current system in the North Atlantic. Major surface and deep-water currents are shown and the study area is highlighted (Nielsen et al., 2007).*

"Changing intensity of the North Atlantic thermohaline circulation, and the consequent north-south shifting of the polar front, is believed to have occurred throughout the Holocene..." (Mcgowan et al., 2008). This assumption is thought to be a key factor for the shifting sea surface temperatures (SST) in the Northern Hemisphere. As a consequence, the SST will effect the Faroese archipelago, because the islands are situated in the center of the inflowing NAC (Amorosi, Buckland, Dugmore, Ingimundarson, & McGovern, 1997; Rasmussen & Thomsen, 2010). During warm periods the Faroes lie in a strong and northward displaced ocean. Unlike cooler periods in the Holocene, the NAC

weakens which result in less warm surface water being carried north. A tongue of polar water from the East Iceland branch of the EGC will therefore approach the Faroes and have an instantaneous impact on the SST. (Mcgowan et al., 2008; Olsen et al., 2010; Humlum & Christiansen, 1998).

2.3.2 Atmospheric circulation system in the North Atlantic

The North Atlantic Oscillation (NAO) is the leading mode of atmospheric circulation variability over the North Atlantic region and is most expressed as the regional weather and climate during the winter season (Pinto & Raible, 2012). The NAO index reflect the state of the NAO, particularly on monthly to seasonal timescales, but can also exhibit decadal and centennial variability. Also, changes in NAO phases are related to surface temperature, precipitation and storm tracks. During a positive NAO phase, a strong meridional pressure gradient, a more zonal flow regime and stronger westerlies, promotes unsteady weather conditions (warmer and wetter) over the central and eastern North Atlantic. This situation is reversed when negative NAO phase occurs (Visbeck, Hurrell, Polvani, & Cullen, 2001). High frequency variability of NAO can be constructed by applying well-dated and annually resolved climate proxies, such as terrestrial and marine records. However, different NAO reconstructions can show disagreements and uncertainties, because proxy records can register different expressions of North Atlantic climate variability (Cook et al., 2019).

2.3.3 Today‘s climate at the Faroe Island

Today, the climate is maritime and is influenced by the warm North Atlantic Current and cooler East Icelandic Current (Andresen et al., 2006; Edwards et al., 2005; Humlum & Christiansen, 1998; Olsen et al., 2010). Accordingly, precipitation in the region is associated to large-scale atmospheric circulation patterns such as the NAO. The average surface water temperatures generates cooler summers and mild winters with mean annual temperature of 6.5 °C in Tórshavn. January is the coldest month with an average temperature of 3.5 °C, while average temperature in August is 10.5 °C (Andresen et al., 2006).

Due to the Gulf Stream in the North Atlantic, the Faroes has 6 to 7 °C higher winter temperatures compared to other places at similar latitudes (Edwards et al., 2005). Although, rapid variations in weather is characteristic for the present climate. The weather is mild, windy, foggy, humid and unsettled (Cappelen & Laursen, 1998). Precipitation is variable across the islands and depends on the local topography and position. Therefore, the average yearly precipitation is less near the coastal regions (about 1000 mm/yr) and more at elevated inland regions (above 3000 mm/yr) (Olsen et al., 2010). The prevailing winds originates from the southwest and can exceed to maximum 43 m/s according to Cappelen and Laursen (1998, p. 35).

2.4 Settlement history and previous studies

The first proposed dates for human activity on the Faroe Islands differ depending on whether palaeoecological, palaeoenvironmental, geological, historical and archaeological methods are employed (Jóhansen, 1985; Arge, 1991; Hannon & Bradshaw, 2000). The traditional view on the first settlers in the Faroes has usually been based on two historical sources; The Færeyinga saga and *De Mensural Orbis Terrae* written by the Irish monk Dicuil (Arge, 1991; Arge et al., 2005). On the other hand, Dicuilt's text regarding the identification of the Faroes has been a subject of debate (Church et al., 2013).

Færeyinga Saga is a collection of various texts, which describes place-names and events that took place in the Faroes. It has thought to be written in Iceland early 1300 century (Arge et al., 2005). The saga and several archaeological sites has considered the major phase of human settlement of the Faroes to be by the Viking Norse expansion during 800-900 AD (Arge et al., 2005; Arge, 2014; Church et al., 2005). The settlers came largely from Norway, although some seem to have had their origins from the British Isles.

The Irish monk Dicuil wrote about the voyages made by Irish hermits in the sea north of Ireland and Scotland (Arge, 1991). The writings is dated back to 825 AD and suggest that a small number of Irish hermits had settled on islands, which in the description points to the Faroes, before the Norse settlement around 700 to the early 900 AD (Church et al., 2005). A supported evidence, are the gravestones on Skúvoy that may indicate a

Hebridean contribution to the islands (Arge et al., 2005). However, there are no remains by hermits on the archipelago, since they were later driven out by the Norse expansion (Edwards et al., 2005). Majority of the archaeological evidence such as written sources, place-names, tradition, genetics supports this view (Arge, 1991).

Studies from the North Atlantic region has gathered evidence of Holocene climate variability (e.g. Arge, 2014; Arge et al., 2005; Church et al., 2013, 2005; Edwards et al., 2005; Gathorne-Hardy et al., 2007; Hannon & Bradshaw, 2000; Hannon, Bradshaw, Bradshaw, Snowball, & Wastegard, 2005; Hannon, Wastegård, Bradshaw, & Bradshaw, 2001; Hannon, Hermanns-Auðardóttir, & Wastegård, 1998; Lawson et al., 2005) mainly from peat, bogs and lakes across the Faroes. In addition, the subject of debate is the connection between the first settlers in the Faroes (establishing the timing) and the vegetation development.

Jóhannes Jóhansen (1985) was one of the first palynological researchers to extensively review the vegetation composition and its evolution in the Faroes, using detailed pollen and plant macrofossils analyses at the sites: Hoydalar, Saksunarvatn, Hovi, Tjørnuvik, Lambi and east of Uldalið at Mykines. He argued that there were pollen evidence for human occupation and his work led him to believe that there were two settlement periods: pre-Viking between 600-700 AD and Viking landnám between 850-900 AD. Several changes in the vegetation history were reflecting human arrival, for instance the detection of pollen *Plantago lanceolata* and the disappearance of *Juniperus* at Tjørnuvik. However, other important indicators were the appearance of *Rumex* pollen. The large quantities of cereal pollen found at Lambi has also been of interest, since it has been suggested as evidence from a pre-settlement period. On the other hand, obtaining reliable radiocarbon dates of the cereal pollen was not possible due to contamination of the material. Instead, Jóhansen collected reliable dates from a peat bog at Uldalið. These radiocarbon dates were interpolated to 650 AD, which proves the onset of cereal growth at Mykines before the *landám* period.

Arge (1991) research points out that Jóhansen‘s investigations of an early settlement could not be supported by archaeological remains, since very few artifacts were dated back

to the early first millennium AD. The Radiocarbon dates from archaeological investigation (e.g. excavations at Toftanes) has supported the traditional accepted chronology for the Norse period, at late 800 AD or early 900 AD (Adderley & Simpson, 2005).

Further archaeological analysis carried out by Church (2013) at á Sondum, Sandoy support the hypothesis that a human colonization occurred at least 300-500 years earlier. Coastal erosion revealed evidence of archaeological remains. A truncated Viking longhouse was dated to the initial Norse colonization 900 AD. However, a sand deposit containing patches of burnt peat ash was also discovered. Samples of carbonized barley grains from these ash patches produced dates during pre-Viking phases, which gives credence to Jóhansen (1985) research. The barley grains are not indigenous to the Faroes and so it must have been either grown or brought to the island by humans. Church (2013) believed that the majority of the remains from early colonization is likely been destroyed by the major Viking colonization, which would explain the lack of evidence.

Hannon and Bradshaw (2000) and Hannon (1998, 2001) replicated Jóhanesen (1985) research. They implied several methods such as plant macrofossils, pollen, charcoal and microtephra analysis to support the radiocarbon datings from the settlement horizon defined as the first pollen instance of cultural disturbance. Their excavations at Tjørnuvik, Eiði and Korkadalur cover the time period before, during and after human interference. Pollen and macrofossil diagrams showed noticeable changes associated with continuous appearance of cultivated crops, charcoal fragments and large Gramineae pollen. The firm evidence were consistent with Jóhannsen (1985) and the calibrated age ranged from 550 to 700 AD (Hannon et al., 2001). The results also show an increase in pollen concentration that may indicate altered catchment conditions or an indirect consequence of human colonization.

The most recent published research on the Faroes is De Wet‘s doctoral dissertation at Lake Eiðisvatn. His well-dated multi proxy records suggest a major environmental disturbance in the lake sediments, which indicates that the humans may have reached the archipelago during 2200 BP (De Wet, 2017). He argues that the marked disturbance seems unlikely to be forced by climatic variability and could rather reflect anthropogenic

factors.

Another debate, is the extent of woodland in the Faroes during the Holocene, specifically pre-settlement period. In the current vegetation there are no trees except for the plantations. However, pollen analysis by Jóhansen (1985) and Hannon and Bradshaw (2000) show traces of tree pollen at Streymoy and Eysturoy. Hannon (2005) dated woody fragments at Heimavatn and the results showed dates from every millennium between 6000 BC and 660 AD. These pollen records can prove that the landscape was partially covered with shrubby woodland vegetation, which were developing into peatland and heathland communities prior to the human settlement. The settlement must have accelerated the vegetation change by the introduction of livestock (Hannon et al., 2005, 2001). However, it is not fully known how much impact the the climate or cultural product had on the vegetation development.

The current evidence for the settlement history in the Faroes varies greatly. However, the development of new methods and techniques are giving researchers more detailed data. For instance, recent radiocarbon dates are currently pushing the earliest settlement of the islands further back in time than traditionally thought (Arge, 2014). Therefore, it is important to re-evaluate previous research. The settlement, called the Norse landnám, is a key feature for understanding the history and the possible human interference in the North Atlantic islands. The Norse landnám occurred in Iceland between AD 870-880 and in Greenland approximately AD 1000 (Church et al., 2005). In the North Atlantic the timing, scale and consequence of human impact varies greatly. Therefore, each archipelago provides opportunity to examine changes on the landscapes (Hannon & Bradshaw, 2000).

3 Methods and Materials

3.1 Field methods

3.1.1 Quaternary geological mapping

To understand and interpret the environmental development in the area it is necessary to collect detailed information about the sediment cover and landforms. The field mapping was conducted with drone images and videos. In addition, a shovel were used for studying the surface sediment cover.

3.1.2 Digital mapping

The presented map in section 4.1 is compiled using a 2 m digital elevation model (DEM) uploaded to ArcGIS 10.5 (Geographic information system). The DEM file is provided by ArcticDEM (Porter et al., 2018). To define the catchment and the drainage system, a watershed flow direction tool is applied from the spatial analyst toolbox. The geomorphology and sediment deposits is recognized using field mapping, drone videos, photos and 3D view in Google Earth. These characteristic features were manually positioned and digitised using points, polylines and polygons from the editor toolbox. Hillshade relief maps and contour intervals were also applied to produce the map.

3.1.3 Piston and Gravity core devices

Coring operation is carried out on a raft and sediment cores were collected with a percussion piston core devise (Nesje, 1992), and a UWITEC gravity core device (Boyle, 1995). Following Nesje‘s (1992) description, the piston corer consists of a corer head with attached wire ropes, sampling tube, stainless piston wire rope, a weight which is lowered and lifted with static ropes, a piston, wire clambs, a core catcher and a jacker. To retrieve the sediments the sampler is lowered down to the sediment surface and hammered until refusal to ensure maximum sediment recovery. The gravity core is limited in terms of gravitational penetration and is ideal for collecting short cores with undisturbed

water-sediment interface.

Before gathering lake sediments for palaeoenvironmental investigations, it is important to acknowledge factors that can cause disturbed sediments (Nesje, Dahl, Andersson, & Matthews, 2000). The topography on the bottom of the lake must be relative horizontal, so that the sediments are being accumulated vertically in the lake basin. It is also crucial that there is little or no resuspension, slumps or turbidites and that the coring takes place away from the in- and outlets to minimize disturbances.

3.2 Laboratory analyses

3.2.1 Sample preparations

All multi-proxy laboratory analyses were carried out at EARTHLAB (Earth surface sediment laboratory) at the Department of Earth Scinence, UiB. The sediment cores was split lengthwise and one half of each core were stored as reference. The working half cores were carefully cleaned and added a scale. Then, visual inspections including colour, composition and layer boundaries were studied in detail. Accurate sampling throughout the laboratory process were essential to achieve reliable results and to limit the source of error.

3.2.2 Radiocarbon ^{14}C dating

Samples were extracted from the piston core sections and rinsed through 125 µm and 63 µm sieves with distilled water. Then, the terrestrial plant macro-fossils were carefully studied under a microscope and fragments for radiocarbon dating was handpicked, dried overnight at 50°C and sealed in sterile glass containers. Two samples with dry weight less than 2 mg were sent to Poznan Radiocarbon Laboratory, Polan and five larger samples were sent to Beta Analytic Inc, Miami Florida. The radiocarbon dates are consistently reported in calibrated years before present (cal yr BP; BP = 1950) according to IntCal13 or "Common era" which is equivalent to AD (CE = 0, suggested birth of Christ).

3.2.3 Age model

The age-depth model was created using the Bayesian framework calibration software called "Bacon" run in R (V. 3.2.2) (Blaauw & Christen, 2013). The data was put in a file containing five columns separated by commas (ID, 14C-ages, error, depth, cc). Moreover, it is essential to specify information before producing the model. The age-depth model was generated by applying the settings: postbomb curve (postbomb=1, representing the North Hemisphere), calibration (cc= 0 or 1, no calibration or IntCal13), length (d.min=0 and d.max=390) and resolution (d.by=1) (Blaauw & Christen, 2011).

3.2.4 X-ray fluorescence (XRF) analysis

The standard procedure starts by making sure that the core surface was flat and covered with plastic to protect the detector. Accordingly, all the LED-01-15 and LEP-01-15 sections were loaded onto the apparatus (ITRAX XRF Core Scanner from Cox Analytical Systems) with the core-top positioned to the right. The scanning is initiated from the software and follows a guided sequence of inputs: Defining the core length, setting the down-core resolution of 500 µm, XRF power settings of 28kV and 25mA, which were applied with a 10 s counting time. To acquire the highest sensitivity of the heavier elements the analysis were performed with a Molybdenum (Mo) x-ray tube. The surface topography scan was used to ensure that the detector and sample distance is monitored and remained constant. The scanning obtains high-resolution elemental abundances from left to right movement of the core, perpendicular to the beam (Figure 5) (Croudace, Rindby, & Rothwell, 2006). Final XRF data are presented as counts per second (cps).

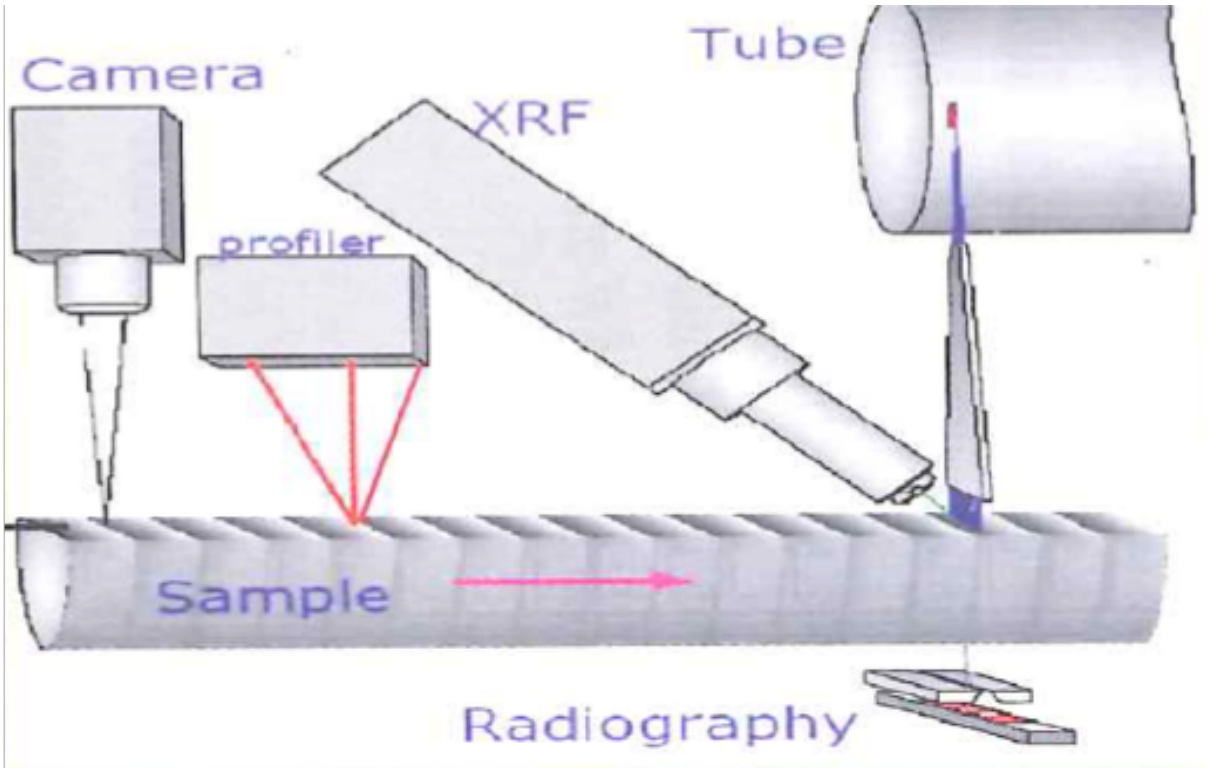

Figure 5: *Schematic illustration of XRF-scanning(Croudace et al., 2006).*

3.2.5 Magnetic susceptibility analysis

Each longitudinal section of the piston core (0-370.5 cm depth) and gravity core (0-158.5 cm) were covered with a plastic film and prepared for magnetic analysis. The apparatus was set at a continuous 0.2 cm intervals with range of 0.1 and sensor type Baertington MS2E point sensor. The instrument consists of four parts (Gunn & Best, 1998):

1. A central sensor array
2. A motorized track that push the core past the measuring sensor
3. An electronic interface transferring data to the logging computer and controlling the sensor settings
4. A logging computer

The point sensor creates a low frequency magnetic field, which measures the degree of magnetic susceptibility of the sample by moving the point sensor of-on contact with the surface. The measurements are commonly presented as unit SI (10^{*-5}).

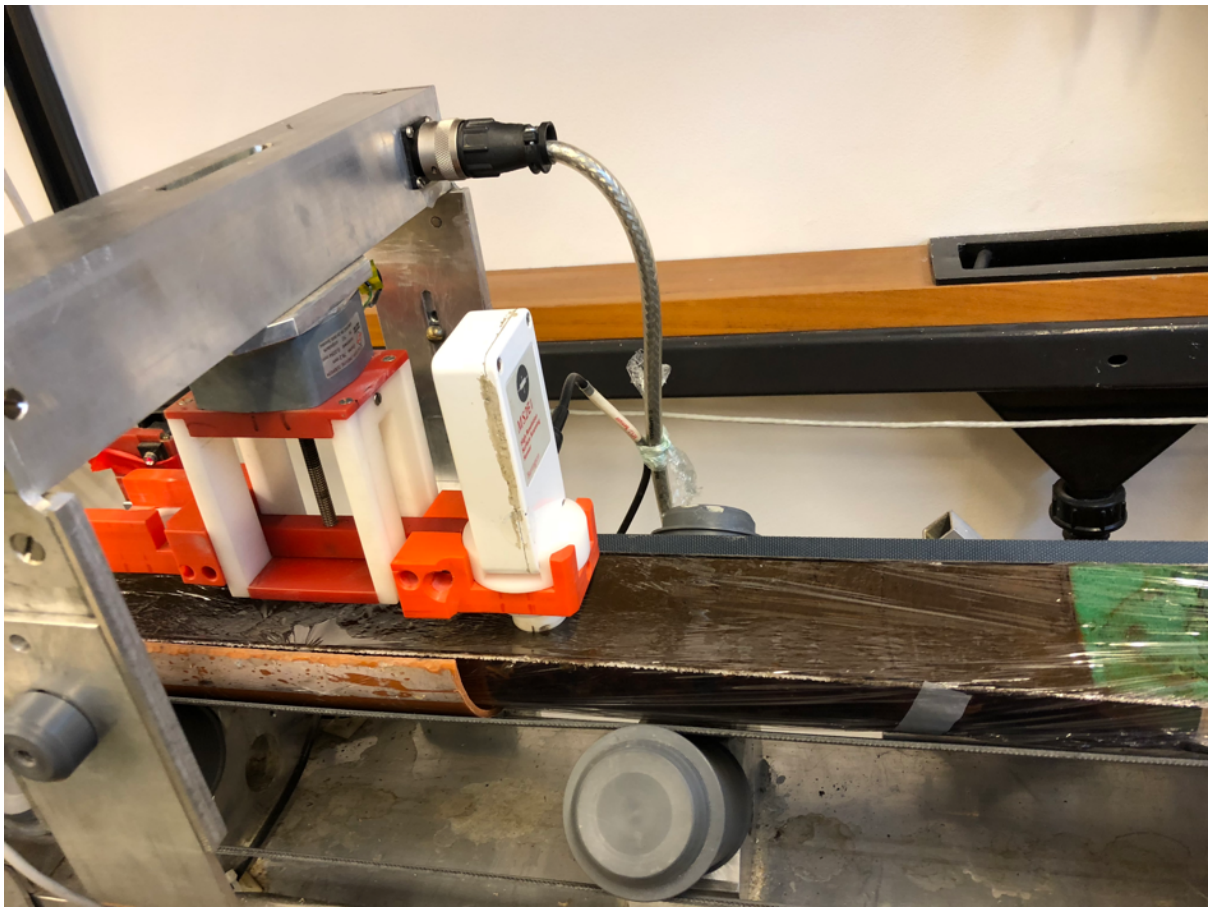

Figure 6: *The point sensor moves up an down of contact with the core surface, which is an important factor when measuring magnetic susceptibility.*

3.2.6 Loss on Ignition

The three LEP-01-15 sections were sampled at continuous 0.5 cm intervals for weight loss-on-ignition (LOI, %) and dry bulk density (DBD, g/cm^3) (in total n=740) following (Dean, 1974) method. Samples were extracted with a syringe to ensure a constant 1 cm^3 and transferred to crucibles. The syringe was cleaned between every sample and crucibles were not touched since it could potentially affect the measurements. The samples were

weighed, dried over night at 105°C, reweighed and combusted for 1 hour at 550°C in a muffle furnance. The samples were put directly into a desiccator and kept there until they had cooled. Note, it is essential that the desiccator is sealed to avoid air or moisture to leak in. Finally, the samples were weighed for the last time. The LOI analysis presented in section 4.4 show an estimate of the weight loss (calculated as a percentage) of the dried sample weight, which reflects the organic content throughout LEP-01-15 core sections. The DBD displays the mass of dry soil per volume unit (g/cm^3).

3.2.7 CT-scanner

Based on the previous laboratory analysis and core observations, a ProCon-X-Ray CT-ALPHA Computed Tomography (CT)-scanning was executed on the two upper sections of the LEP-01-15. The apparatus was set at 120kV and 800 uA, creating 54.1 µm vokel resolution with exposure time of 267 msec. The instrument detects a three-dimensional internal visualization of the sample, sediment structures, density variation and shape of both split and whole cores (Cnudde & Boone, 2013). During the operation the core is installed vertically on the core holder, which has a rotational movement around its vertical axis. The x-ray source and detector system remains in position, moving up and down the core. This way a number of different angular scanning images are made. X-rays are emitted by a source and absorbed and scattered by the sample before detected. To prevent increased absorption in the outer region of the sample, an X-ray compensator (1 mm aluminum filter) was applied to attenuate the low- energetic (soft) x-rays. Additionally, reconstructing scans and data processing were proceeded with the FEI Avizo 3D software.

4 Results

4.1 Quaternary geological mapping

During fieldwork conducted in June 2018, a variety of geomorphological features and Quaternary sediments were found. These features can be divided up into following groups: slope deposits, fluvial deposits, peat cover and erosion channels. The sediment deposits are connected to different types of processes with numerous ages and origin. Therefore, they are crucial for identifying potential sediment sources for the sediments found in the lake basin. A simple Quaternary geological map of Leynavatn (Figure 8) and a digital terrain model analysis (Figure 7) is generated based on methods in section 3.1. Note, that the entire catchment is not fully mapped in detail.

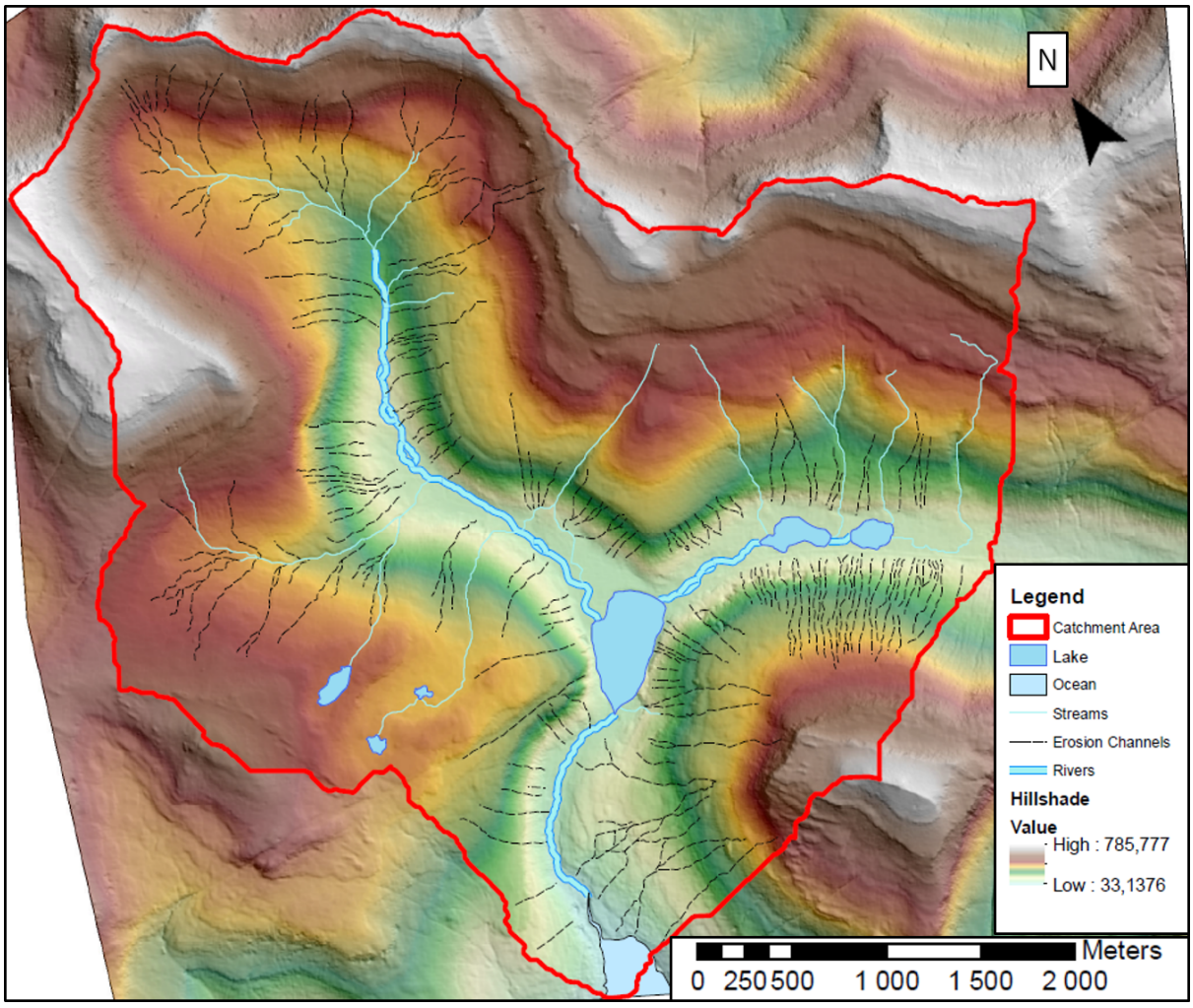

Figure 7: *A simplified terrain model of the Leynavatn catchment. The catchment is outlined by a red line and includes major streams, rivers, lakes and erosion channels.*

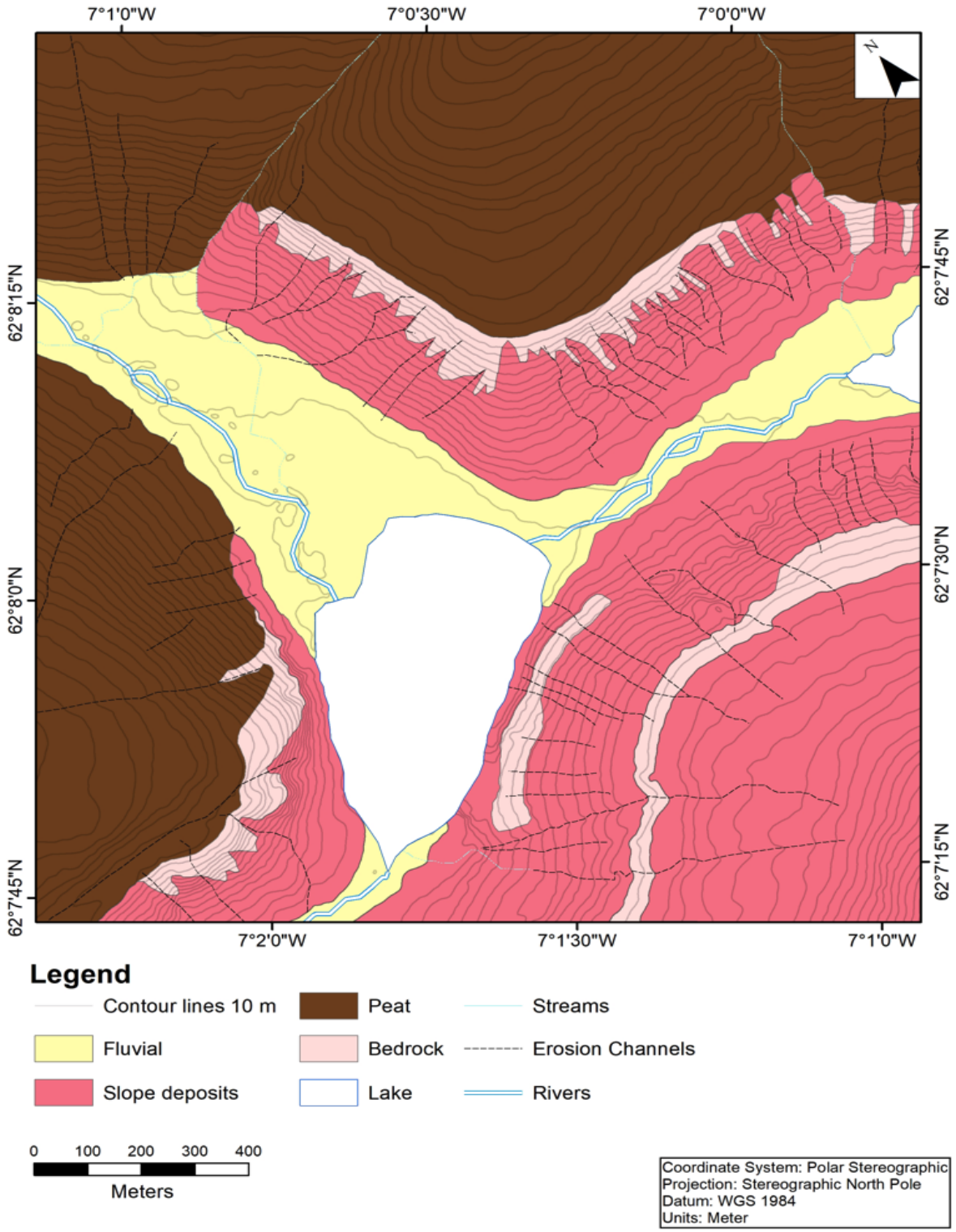

Figure 8: *A simplified Quaternary Geological map of Leynavatn showing different deposits acting in the area today. The legend show different color shading reflecting type of sediment cover.*

4.1.1 Glacial features

Observation: Several mountains and narrow ridges with an altitude between 400-500 m a.s.l. create well developed U-shaped valleys. The valleys exhibit different slope gradients with steep upper slopes (between 60-30 degrees) that becomes gentle towards the valley floor.

Interpretation: During the last glaciation, the Dalá valley (located north of Leynavatn) contained a southward-flowing glacier that eroded the landscape (Guttesen, 1996). As a result, the surrounding landscape was covered by loose unconsolidated sediment. Later on, enormous quantity of material was removed by surface drainage and formed an U-shaped valley. No glacier deposits are found during the field work, although sediments are likely to appear under the peat cover away from the drainage paths. Farther in the Dalá valley the presence of a glacier is indicated by tall peaks (around 700 m a.s.l), aretes and cirques.

4.1.2 Gravitational slope features

Observation: On the mountain slopes surrounding Leynavatn there is several material accumulation features. Especially the mountain west of the lake basin hosts cone shaped deposits, which are coalescing with one another (Figure 9). These are a couple hundred meters long, c. 200 m and consist of fine sand to rock. Prominent channels overlying the thin vegetation cover are also found on the mountain slopes. In addition, numerous large fractions of rock varying in size (less than 2 m) are moving downslope within the finer vegetation cover and terminates at the lake shore.

Interpretation: The gravitational slopes deposits are classified as colluvial fans (Blikra & Nemec, 1998) and can also be determined as a colluvial apron. The surface of the larger fans have been reworked by several processes including slope wash and rockfall and imply that the colluvial aprons is still active. Also, avalanche deposits including rockfalls, rockslide and debris flows and some occasionally slides of rock or debris have

been a common occurrence throughout the area (Figure 9). Hence, the erosion processes is complex and the combination of geology, geomorphology, relief and weathering creates a dynamic landscape (Blikra, 1990).

Figure 9: *From Leynavatn in Streymoy, southeast Faroe Islands, an area with high activity of downslope processes, which develops erosional channels, colluvial fans and rockfall deposits.*

4.1.3 Fluvial features

Observation: Gravel-sand beaches are observed near the two river mouths, at the northern and eastern side of the lake. Note, that the two inlet rivers runs through separate valleys before entering Leynavatn. The outlet river runs from the southwest end of the lake towards the sea (Figure 10). The first inlet river has a meandering appearance and runs in north-south direction (Figure 11). While the second inlet river runs from east-west direction and is the outlet from Vestara Mjáavatn (Figure 12). Sediments of all fractions, clay-pebbles with rounded shapes are found. Also several active, semi-active

(only active during high precipitation), and passive fluvial channels of variable sizes, are evident on the surrounding mountain slopes.

Figure 10: *The outlet river "the Leynára" follows the topography and flows towards the ocean.*

Interpretation: The rivers and streams are crucial landscape features at the Faroe Islands, due to the high precipitation levels (Mcgowan et al., 2008). Fluvial drainage paths transport important mineral particles and allochthonous materials from the surrounding soils and bedrock, which is then deposited in the lake basin. Thus, the relation between the catchment and the lake is an important factor that effects the sedimentation rate, because the streams connects different areas of the catchment with the lake.

Figure 11: *The main inlet river "Dalà River" transports allochthonous materials from the catchment to Leynavatn. The river is a crucial landscape feature due to the high precipitation and surface runoff.*

Figure 12: *The outlet of Vestara Mjáavatn entering Leynavatn.*

4.2 Coring

In August of 2015, four lakes were cored in total, Eidisvatn, Leynavatn, Sandsvatn, and Grothusvatn. During this campaign a team from University of Bergen and University of Massachusetts Amherst recovered two sediment cores from Leynavatnet (Figure 13) A gravity core:(LED-1-15; 0-158.5) and a piston core: (LEP-1-15: 0-108 cm; LEP-1-15: 108-253 cm; and LEP-1-15: 253-370.5 cm), which were divided up into three sections to allow for transport and core scanning. All the cores were packed for shipment and sent to the University of Bergen for splitting and laboratory work.

Table 1: *Overview of sediment cores collected from Leynavatnet*

Core Identifier	LED-1-15	LEP-1-15
Core Type	Surface/Gravity	Piston
Core Length (cm)	158.5	370.5
Location	62.12777° N 07.024623° W	62.12777° N 07.024623° W

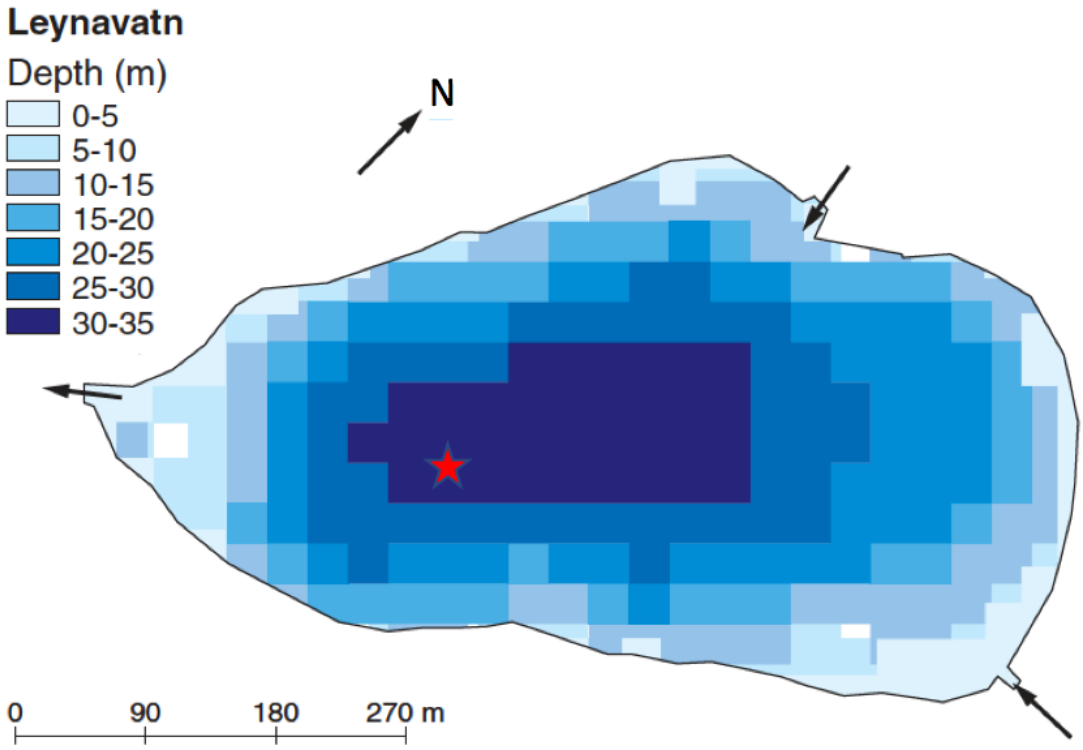

Figure 13: *Bathymetric map of Leynavatn modified from (Landkildehus et al., 2002). Red start marking the coring location at c. 30 m water depth and arrows showing important outlet and inlet rivers.*

4.3 Chronology

4.3.1 Radiocarbon dating results

Firm chronology has been established for the composite sediment record based on Accelerator Mass Spectrometry (AMS) radiocarbon dating of plant macrofossils (see table 2).

Generally, lakes accumulate material derived from within and outside the lake basin.

Table 2: *Radiocarbon dates from (LEP-01-15) and core surface from (LED-01-15), Leynavatnet.*

ID	Cores, Sections	Depth (cm)	Sample	Conventional ^{1}4C-age (BP) with Error	Calibrated Age Range (2σ)(yr BP) 95.4% Probability	D^{1}3 C (‰)
Core Surface	LED-01-15	0		Modern	-65	
Beta-512660	LEP-01-15, 1	12	Plant macrofossil	105.76 ± 0.39 pMC	-56–60	-26
Poz-110010	LEP-01-15, 1	79.8	Plant macrofossil	940 ± 30		
Beta-512661	LEP-01-15, 1	104.5	Plant macrofossil	550 ± 30	564-516 639-591	-26.3
Beta-512662	LEP-01-15, 2	150	Plant macrofossil	640 ± 30	610-554 668-621	-22.3
Beta-512663	LEP-01-15, 2	202.5	Plant macrofossil	690 ± 30	685-638 592-562	-24.7
Beta-512664	LEP-01-15, 3	290.5	Plant macrofossil	1140 ± 30	1096-969 1148-1102 1174-11158	-24.5
Poz-110012	LEP-01-15, 3	349	Plant macrofossil	1375 ± 30		

4.3.2 Age models

Bacon age-depth modeling uses bayesian statistics to build an age-depth relationship. The model breaks the composite depth into a given number of subsections and runs simulations for each of them with the prior assumption that the age should increase with depth. This way, the curve is fitted to the radiocarbon data and interpolated to obtain an age estimate for all depths of the composite record. The prior information is based on Table 2. It is not unusual that dates can appear to be inverted, which one needs to

take into account. Therefore, two different age models were created. The first model "LEP" (Figure 14) utilize all available radiocarbon dates to determine which dates are true outliers, while "LEP1" (Figure15) excludes the possible outliers. Figure (15) is used to plot all proxy data in this study.

Sediment accumulation rate (SAR) for both models is calculated with the median age. The SAR vary between 0.15-0.45 cm/yr. An abrupt change in SAR is recorded at 124-222 cm shown in Figure 14. In contrast, Figure 15 only shows this distinct interval between 170-222 cm. Hence, the rate throughout the composite depth is generally around 0,25 cm/yr.

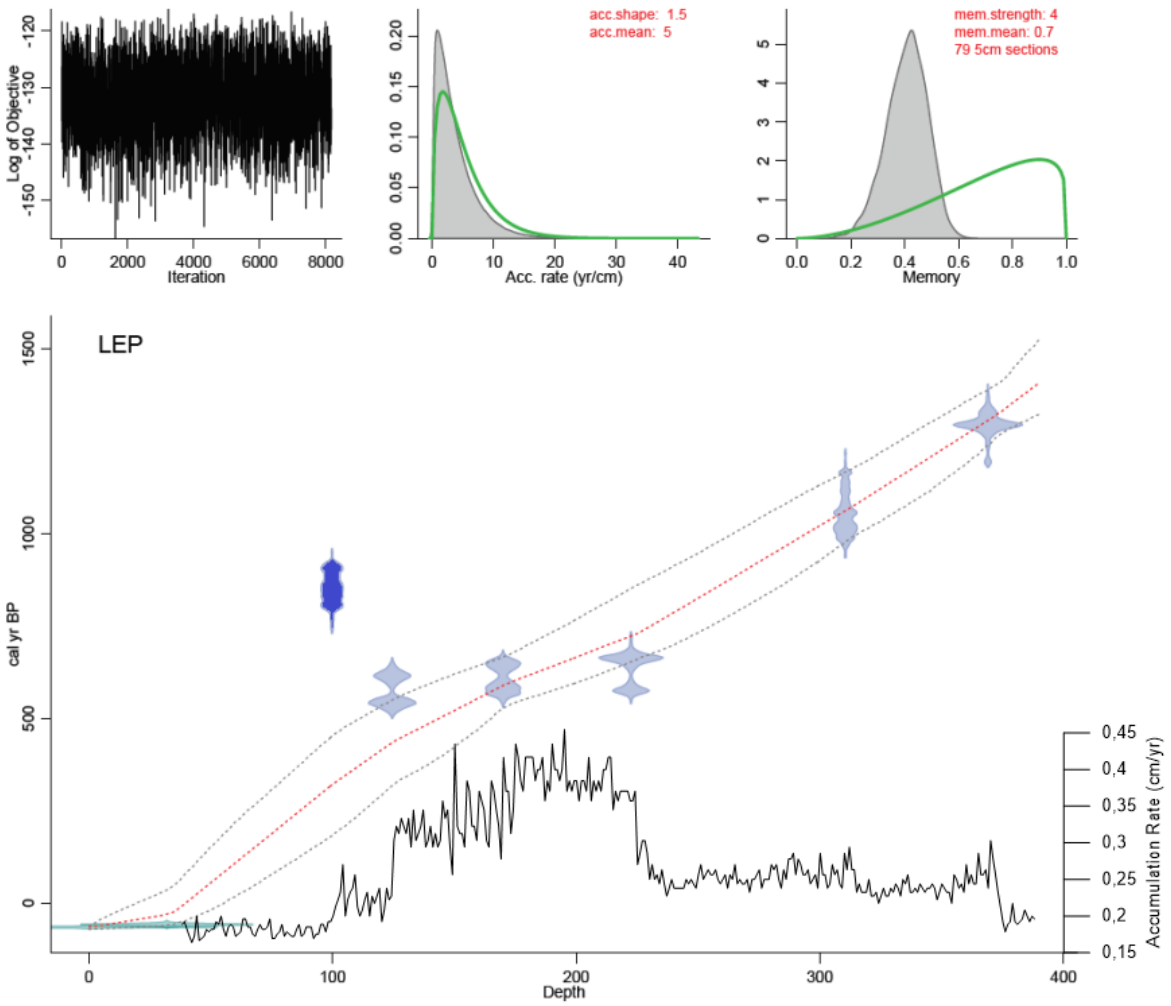

Figure 14: *LEP-01-15 age-depth model created with software Bacon using all available radiocarbon ages (blue symbols) and surface sediments (turquoise symbols). Possible outlier (dark blue symbol); The computed age depth curve (dashed red line); Curve estimates of the model uncertainties (dashed grey lines); Sediment accumulation rate (bottom panel). Note, the parameters that constrain the model are on the top of the figure.*

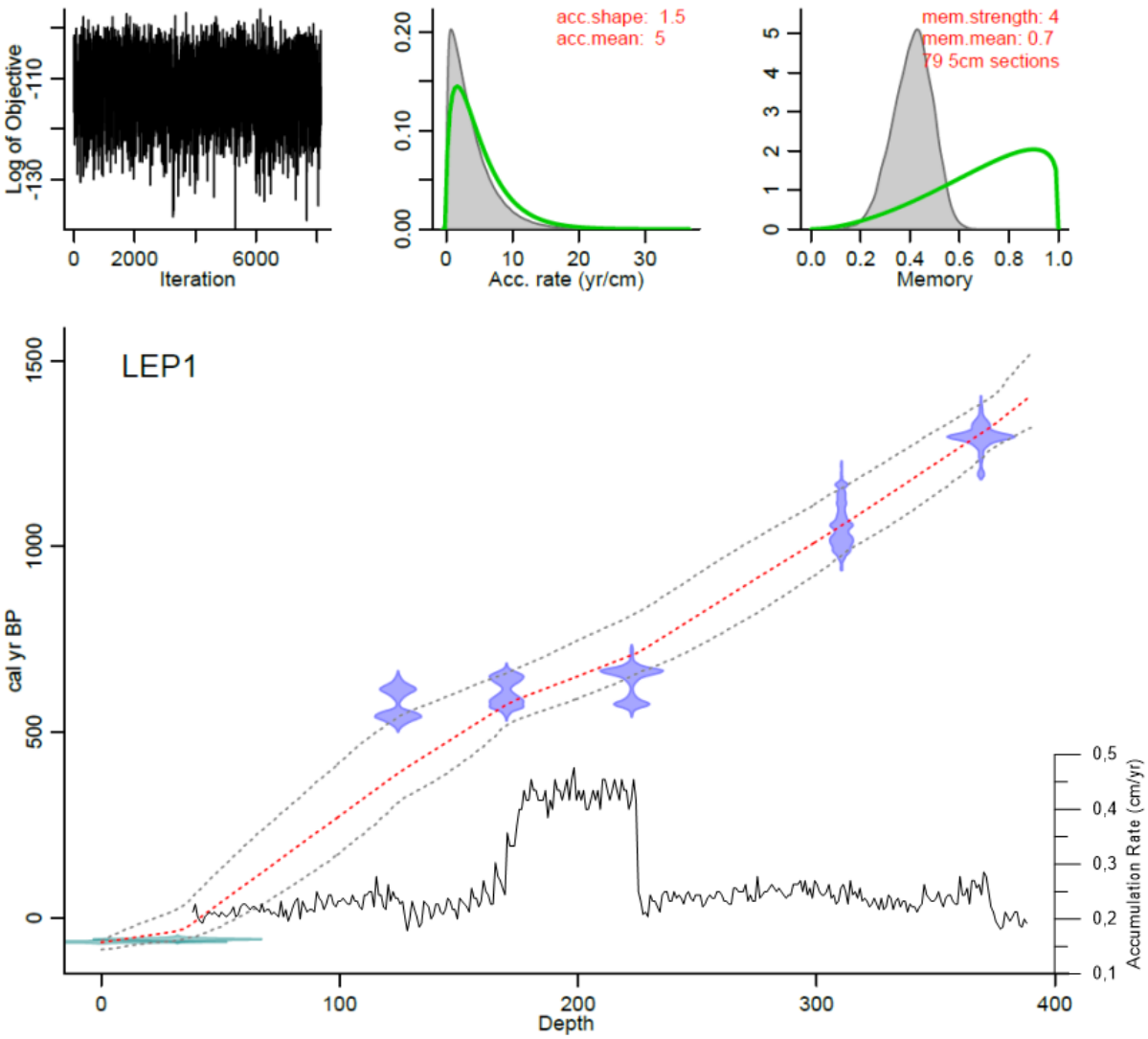

Figure 15: *LEP1-01-15 age-depth model created with software Bacon and without inverted dates. Conventional radiocarbon dates (blue symbols); Surface sediments (turquoise symbol); The computed age depth curve (dashed red line); Curve estimates of the model uncertainties (dashed grey lines); Sediment accumulation rate (bottom panel). Note, the parameters that constrain the model are on the top of the figure.*

4.4 Sedimentary properties

To identify the number of significant lithological units a composite sediment record is constructed by correlating magnetic susceptibility gathered from the piston- and gravity cores. The relative displacement of the top sediments on both cores were determined (Figure 16) and illustrate that the cores align. However, the piston core is missing the upper 20 cm of the composite sediment sequence (Note that the LED-01-15 is stretched out for comparison). This results in a 390 cm composite record.

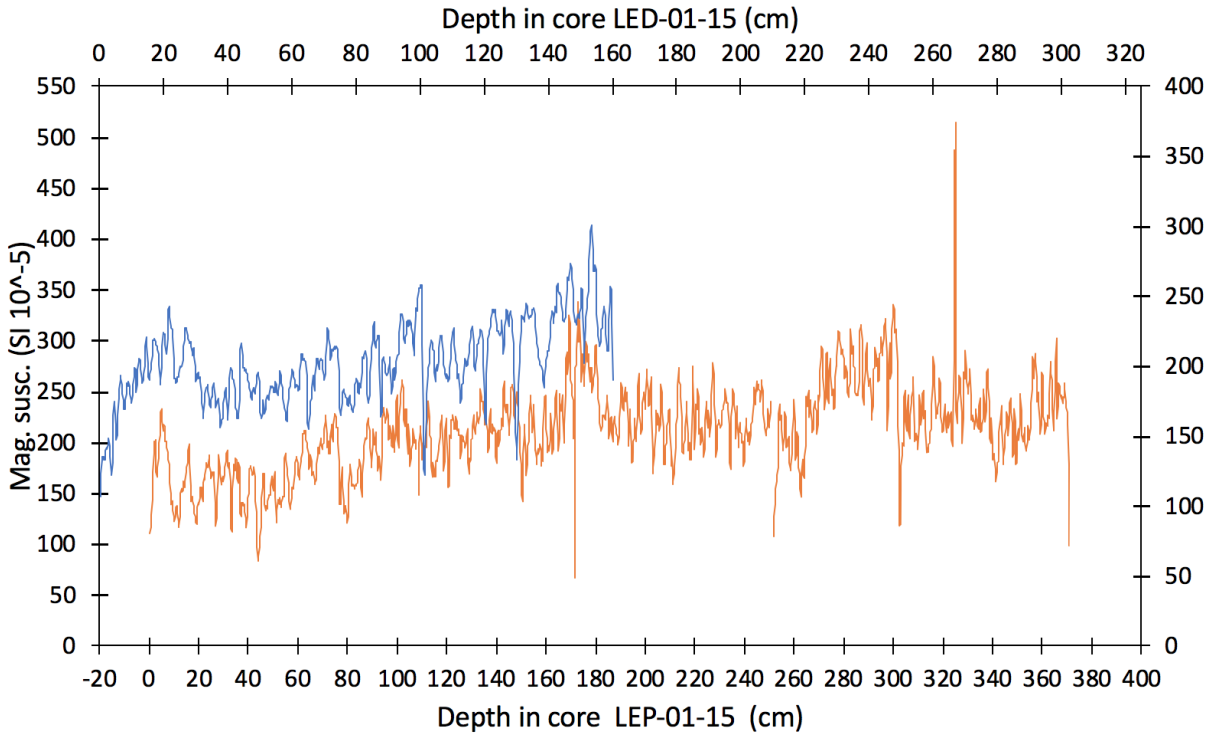

Figure 16: *The LEP-01-15 (orange) plotted next to LED-01-15 (blue) to show variability in magnetic susceptibility. The plot illustrates that the LEP-01-15 is missing 20 cm of the top sediments.*

In addition, the cores were used to characterize the 8 units. Figure 18 defines all the units based on LEP-01-15, while LED-01-15 shown in Figure 19 includes the units: A, B, C, and D (all the depths in the following chapter are expressed as centimetres below water surface). Down-core variations in visual stratigraphy, LOI (detecting shifts in

organic productivity or preservation), DBD (variations in bulk dense material input), MS (reflecting inorganic catchment derived input), CT (characterize variations in density, detect particles and sediment structures) and XRF (capturing shifts in geochemistry) is applied to distinguish the units. Note, that some images can deviate with the proxy data and that the collected raw data is smoothed with a running average (red profile lines).

4.4.1 Core description and multiproxy results

Unit H: LEP-01-15(370-341 cm): The bottom part of LEP-01-15 is defined as unit H and consist of a dark grey and brown gyttje (10YR 2/2 Munsell chart value (Munsell & Color, 2000)). The Loss-on-Ignition (LOI) raw data is low, minimum 10.3 % at 365 cm depth. At the same depth, the dry bulk density (DBD) values are high, maximum 49.2 g/cm^3. Notice, that the variation in DBD is correlated inversely with the LOI record. At 353 cm depth the LOI increases to 15 % and DBD decreases to 38 g/cm^3. The geochemical elements also fluctuate within the unit and the Fe profile slightly decreases to 67809 cps towards the transition to unit G. The Ti counts decreases 3323 cps at 353 cm depth. Thus, the Incoh/Coh scattering ratio show related profile characteristics with the LOI. The x-ray image display clear light and darker layers, which reflects the density variations in the unit. In addition, the surface magnetic susceptibility (MS) values changes from maximum 301.7 SI to 161.2 SI upwards in the unit.

Unit G: LEP-01-15(341-302 cm): Unit G consist of faint laminations of silty gyttja (10YR 2/2), with high content of organic material and scattered rust stains on the core surface. At the transition into G, the MS values are increasing and peaks (550 SI) at 325 cm depth. Thereafter, the MS decreases to 120.3 SI towards the next unit F. Note, that a small rock is found at the core surface at 325 cm depth(Figure 17). In contrast, the LOI, DBD and geochemical elements are variable, where the LOI has smaller fluctuation intervals with minimum and maximum percentages of 10.1 % and 14.9 % and the DBD changes between 38.6-45.3 g/cm^3. The Ti, Fe and Incoh/Coh ratio counts show fluctuations with smaller amplitude than the LOI results. At depth 303 cm a distinct

black low density layer appears on the optical and radiographic images. The layer is 1.5 cm thick and marks the transition to the unite above, since the color is different(5YR 2,5/1) and the layer consist of organic material (Figure 18). The geochemical elements and the MS also reply with a marked spike, where Ti is 1727 cps, Incoh/Coh is 5 cps and MS is 118.9 SI.

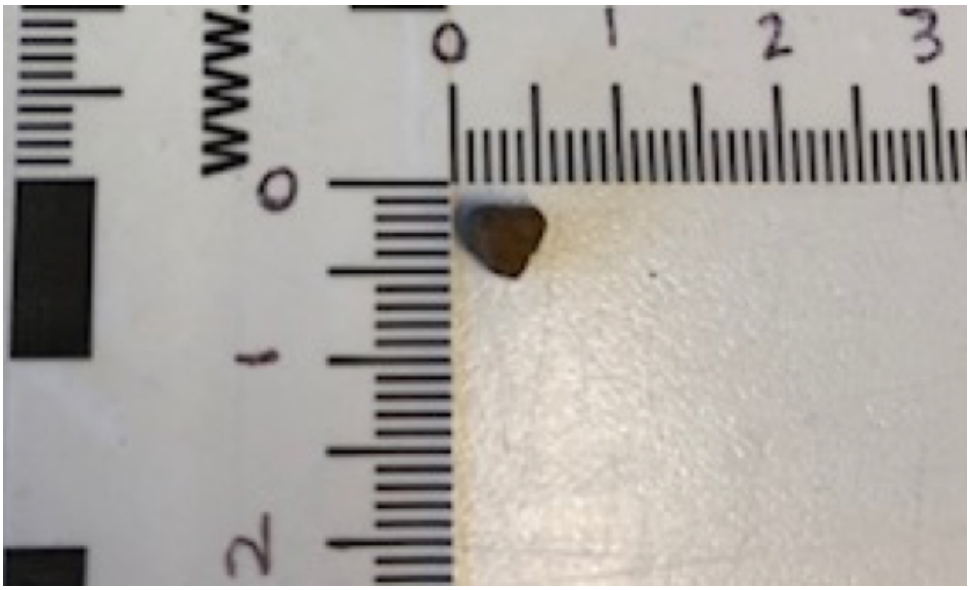

Figure 17: *0.5 cm rock found just below the core surface at 325 cm depth.*

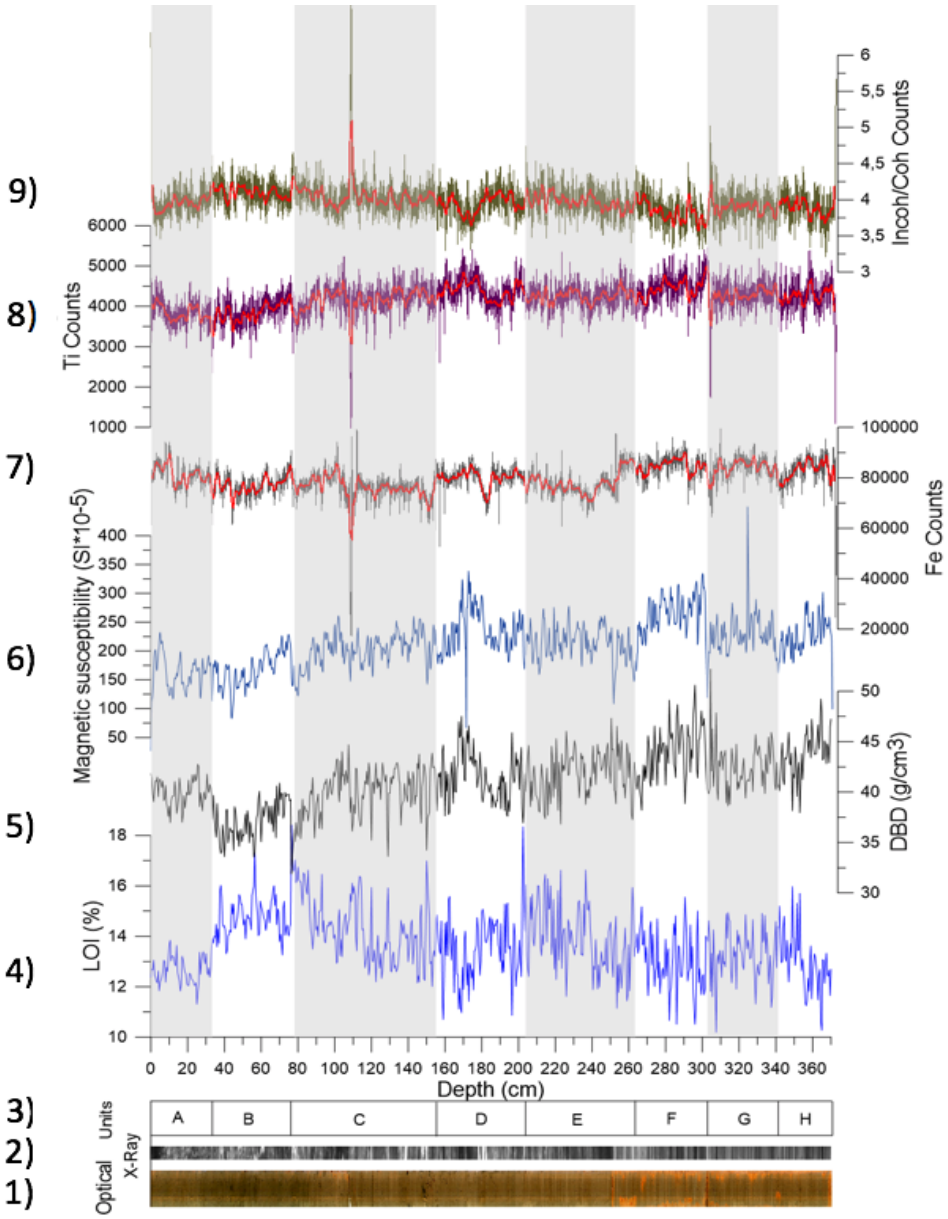

Figure 18: *Selected magnetic, physical and geochemical properties of LEP-01-15. From left to right: 1) Optical core image of LEP-01-15; 2) Radiographic image; 3) Units (A-H); 4) Loss-on-ignition (blue line); 5) Dry bulk density (black line); 6) Magnetic susceptibility (dark blue line); 7) Iron (dark grey line); 8) Titanium (purple line); 9) Ratio between incoherent and coherent scattering (geen line). Note, all the geochemical proxies include a 35-point running average (red line) and that the different units are outlined with white or grey background color.*

Unit F: LEP-01-15(302-263 cm) Unit F shows faint light and dark brown laminated layers with sediments consisting of clay to fine sand. Traces of organic materials, such as peat is distinctive. The unit has a sudden increase in surface MS 334.6 SI, which is prolonged until 272 cm depth. The prolonged high MS is reflected by small fluctuating intervals in geochemical elements, LOI and DBD, where Ti counts are between 3253-5308 cps, Incoh/Coh ratio between 3.3-4.5 cps, LOI between 10.5-15.5 % and DBD between 38.8-50.6 g/cm^3. After 272 cm depth the MS decreases to minimum 147.2 SI, which defines the next transition to unit E. The LOI and Incoh/Coh ratio increase at 270 cm depth to maximum values of 15.9% and 4.5 cps. Proxy changes throughout the unit corresponds with the lamination's shown in the radiographic image.

Unit E: LEP-01-15(263-203 cm) This unit is characterized by very fine sediments(5YR 3/2) with organic material. This is reflected by a increasing trend in the LOI, with maximum value of around 18 % at 202 cm depth. However, the trend is interrupted by smaller fluctuation intervals in LOI where lower percentages (less than 12 %) are found at 253 cm, 243 cm, 226 cm and 220 cm depth. Thus, the MS and geochemical elements exhibits several small fluctuations throughout the unit, which can be related to the laminations shown in Figure 21b.

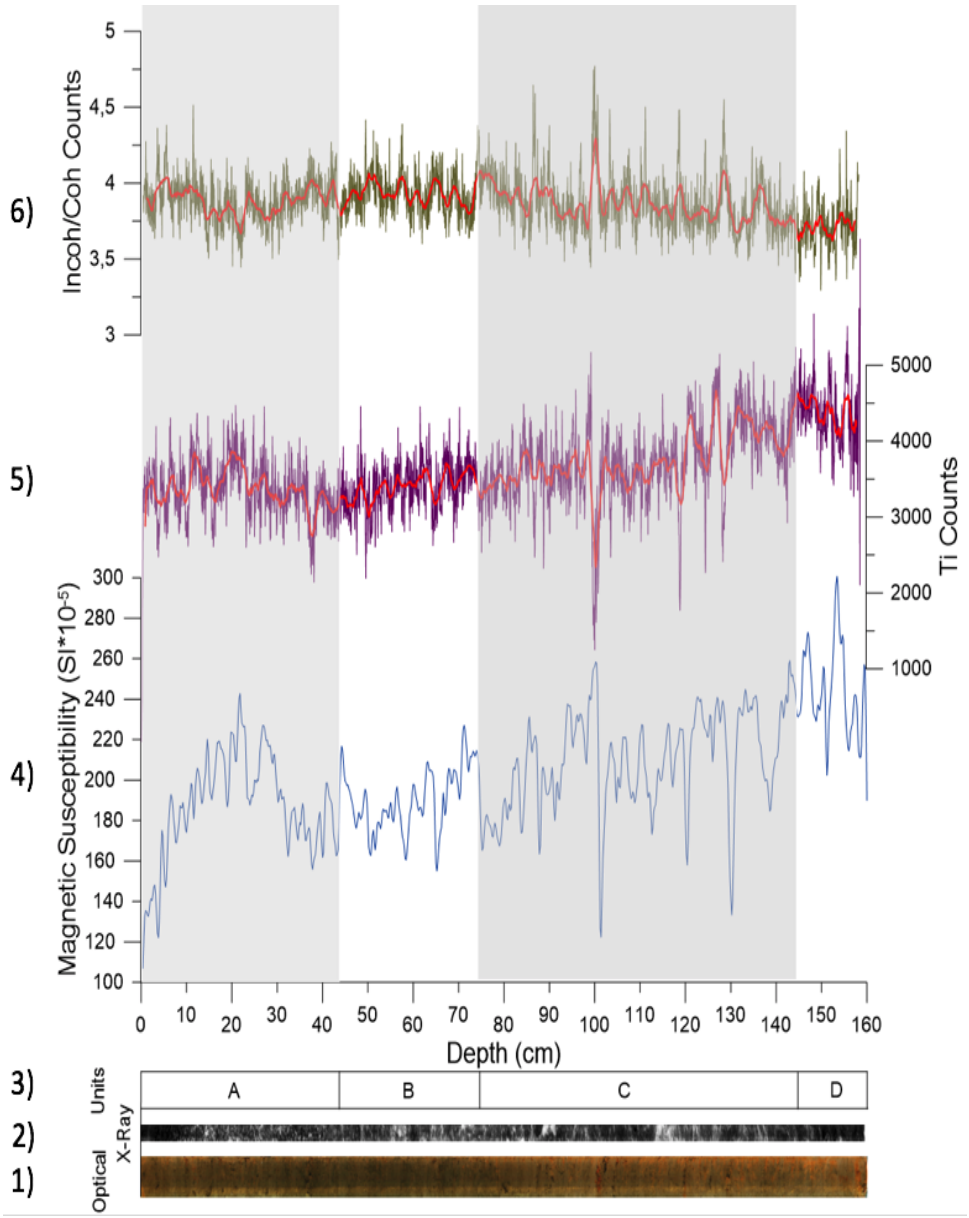

Figure 19: *Selected magnetic, physical and geochemical properties of LED-01-15. From left to right: 1) Optical core image of LED-01-1; 2) Radiographic image; 3) Units (A-D); 4) Magnetic susceptibility (blue line); 5) Titanium (purple line); 6) Ratio between incoherent and coherent scattering (geen line). Note, all the geochemical proxies include a 35-point running average (red line) and that the different units are outlined with white or grey background color.*

Unit D: LEP(203-159 cm) & LED(158-139 cm) Unit D has laminated sandy silt with millimetre to a few centimetre sized organic material. The distinct laminations have different densities and are detected on the x-ray and CT-images. The radiograhic image defines high densities as dark lamination and opposite for lower densities. In contrast, the CT image (Figure 21b) display sand sized particles as yellow and pink. Between 182-192 cm depth, Ti, DBD and MS show similar trends, where they decrease to minimum of Ti 3055 cps, DBD 37.5 g/cm^3 and MS 194.6 SI. In contrast, the LOI and Incoh/Coh ratio has a increasing trend of maximum 15 % and 4.4 cps. However, at 182-165 cm depth, a distinct peak derived by increasing Ti 5429 cps, DBD 47.5 g/cm^3 and MS 338 SI. Unlike the other proxies, the LOI decreases to a minimum of 11%.

The upper part of unit D can also be found at the base of LED-01-15 (shown in Figure 19). The highest value of MS 300 SI can be traced at 153 cm depth. The Ti profile also exhibits high count rates, maximum 5750 cps, while the incoh/coh scattering show the lowest count of 3.2 cps at 150 cm depth. Although both the Ti and Incoh/Coh ratio fluctuate with interrupted smaller intervals.

Unit C: LEP(159-76 cm) & LED(139-75 cm) Unit C consist of dark brown, silty, sediments with organic material (10YR 2/2 and 7.5YR 2.5/2). Approximately, 2 cm long macro fossils are found. Throughout the unit there is a lengthened decreasing trend in the MS from 146-80 SI (smaller fluctuations within the interval). The opposite is observed for LOI, which increases 11% in the lower part of the unit to more than 18% in the uppermost part of unit C (opposite for the DBD). However, an abrupt change in the geochemical elements occur at 108 cm depth, were the Ti and Fe decreases to 1021 cps and 19304 cps.

LED-01-15 show similar trends as LEP-01-15. The decreasing trend in MS has prominent fluctuation intervals where minimum values are more distinct at depths: 133 cm, 120 cm and 102 cm. These minimum MS results are reflected in the geochemical elements as decreasing Ti counts and increasing incoh/coh ratio. At the mentioned depths the Ti is 2411 cps, 1770 cps, 1249 cps and Incoh/coh is 4.5 cps, 4.4 cps, 4.7 cps.

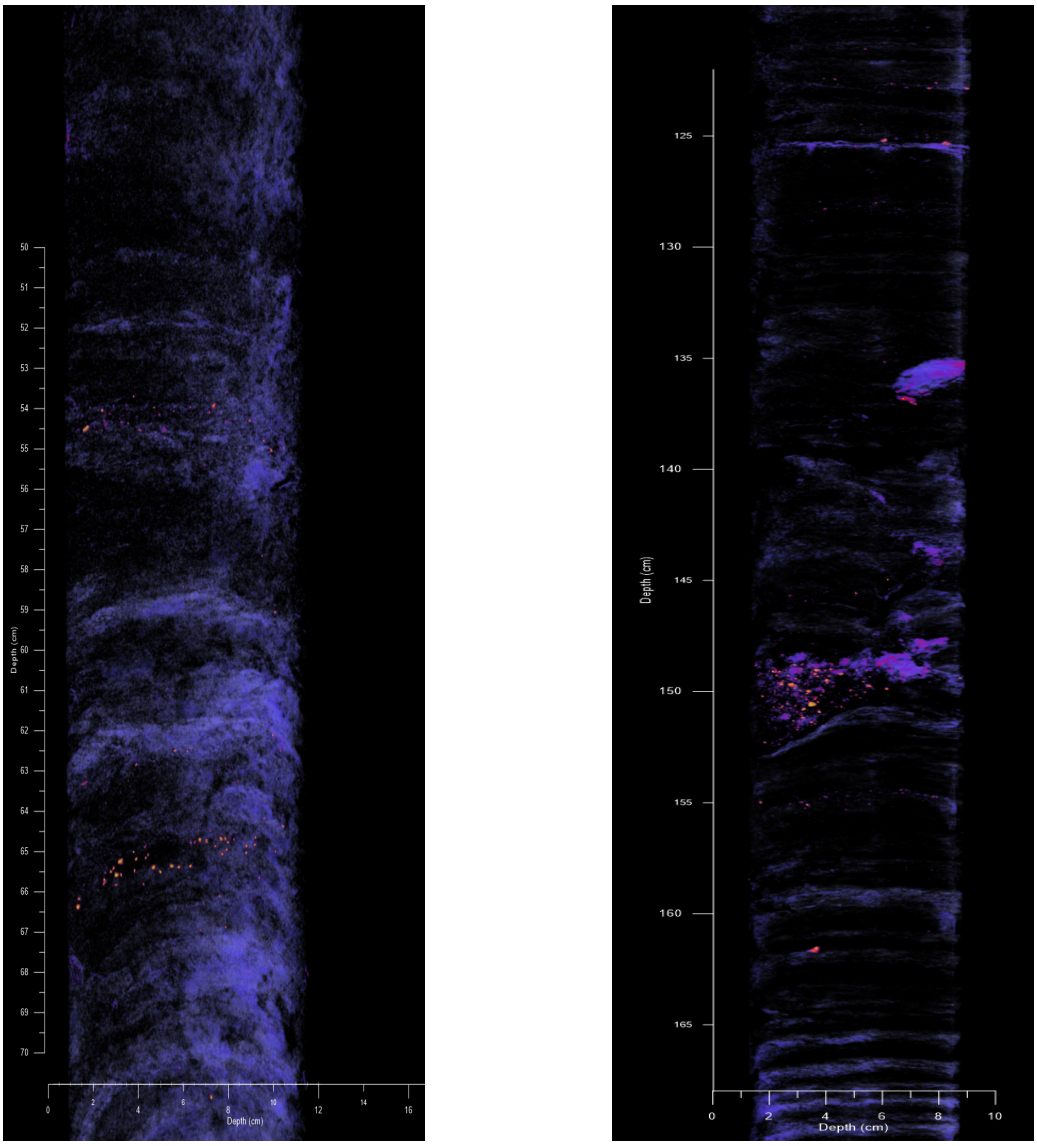

(a) *Section 1* (b) *Section 2*

Figure 20: *Selected segments from LEP-01-15 showing layers with distinct particles gathered from the X-ray CT analysis. A) Represents 50-70 cm of section 1 LEP-01-15 and show two distinct horizons where particles are visible at around 65 cm and 54 cm depth. B) Represents 120-170 cm of section 2 LEP-01-15 and high concentration of particles is visualized with purple, pink and yellow colors at 150 cm depth.*

Unit B: LEP(76-33 cm) & LED(75-43 cm) The unit B is distinguished by the maximum value of LOI 18 % (and lowest DBD) at 76 cm depth and minimum value of 12 % at 33 cm depth. The upper transition is also defined by lower count rates in Ti 521 cps and Fe 61448 cps. Throughout the unit the MS changes with small fluctuation intervals with a decreasing trend. Thus, a change in the radiographic image illustrate that the sediment is not clearly laminated compared to the units below, although the CT image Figure 20a show distinct particles found in matrix-supported layers at 65 and 54 cm depth. Visual observations show similar characteristics as unit C.

The LED-01-15 show distinct intervals where the magnetic properties is persistent with smaller fluctuations. The geochemical elements reflects these changes.

Unit A: LEP(33-0 cm) & LED(43-0 cm) The top part of LEP-01-15 and LED-01-15 characterize unit A. Reddish brown sediments (7.5YR 2.5/2) dominate the upper unit A in LEP-01-15. The sediments varies from fine silt to sand. Low LOI 12.3 % and slightly high DBD 39.7 g/cm^3 at the base of unit A defines the boundary between unit B to A. Further, smaller fluctuation intervals in the MS and the geochemical elements. The radiographic and CT image A (Figure 21 illustrate that the sediments are not fully laminated.

The 20 cm of sediment that is missing in the LEP-01-15 appear in the in top part of LED-01-15. The magnetic susceptibility is decreasing from 240-110 SI (corresponding depth: 20-0 cm), followed by geochemical elements fluctuating, where maximum and minimum counts for Ti between 4287-2245 cps and Incoh/coh between 4.6-3.5 cps within unit A.

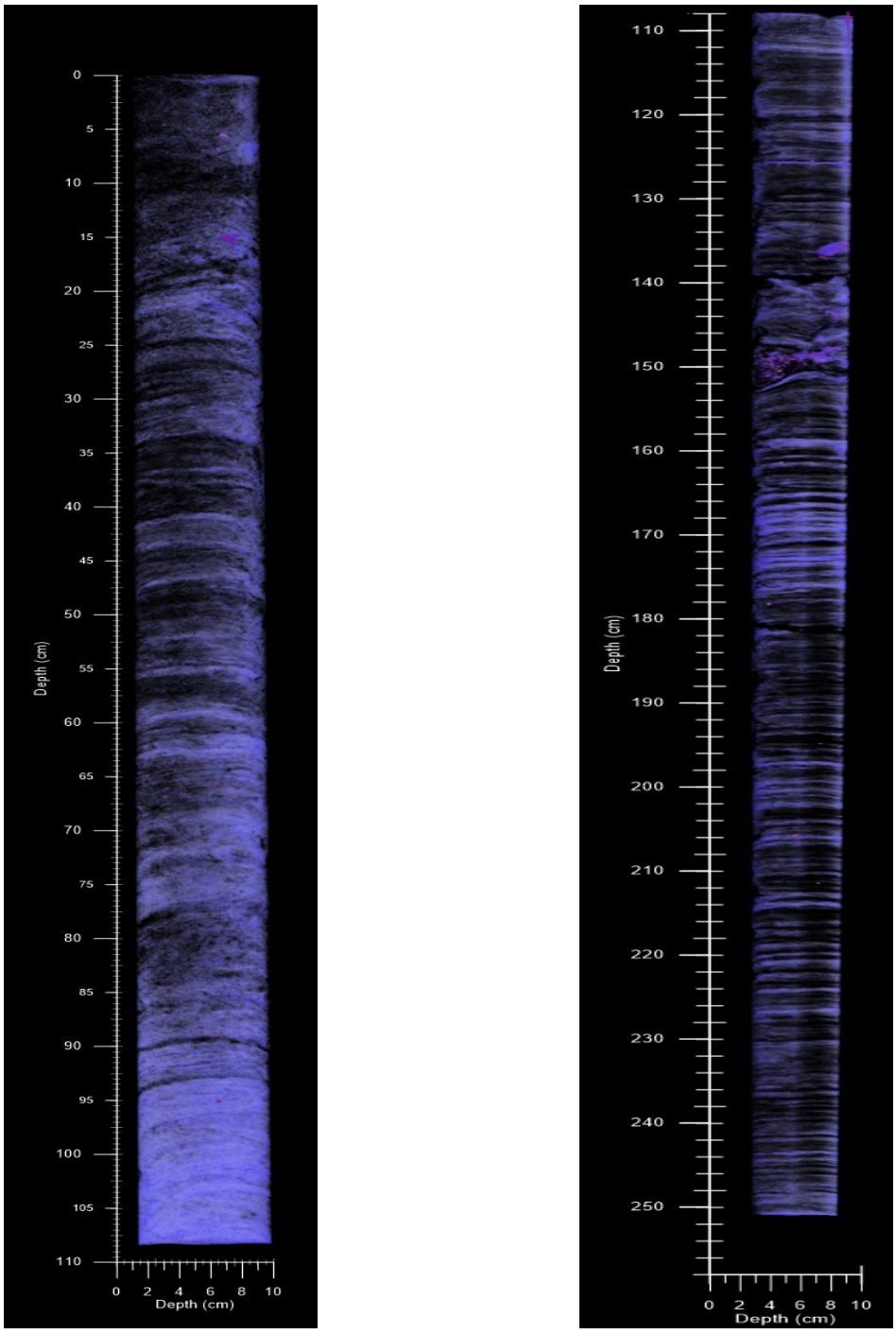

(a) *Section 1 (0-108 cm)* (b) *Section 2 (108-253 cm)*

Figure 21: *Results from the CT-scanning performed on the two upper section of LEP-01-15. The changes in detrital input can be viewed on the greyscale values are shown from black (low density) to yellow (high density).*

5 Discussion

5.1 Geomorphologial setting

The interaction between climate, vegetation and human activity is important to understand before identifying climate signals from lake sediments. Although, the geomorphology and topography within the Leynavatn catchment must also be considered. The catchment processes relates to the maritime nature of the climate such as extreme events and storminess. Slopes and grounds are continuously being exposed for high erosion and slope wash. As a consequence, landforms are reshaped and gravitational mass movements depositing colluvial aprons, rockfalls and debris flows is evident. During high precipitation periods, an increased transport efficiency of inflowing rivers and streams will deliver distant sources within the catchment to Leynavatn. As a result, the large catchment will be more sensitive and allochthonous materials will highlight patterns of landscape instability.

5.2 Interpretation of Leynavatn sediment record

The radiocarbon analysis shows that the Leynavatn sediment record only covers the late Holocene, since the oldest date is 1375 ± 30 cal. yr. BP (Table 2). Also, it reveals particularly high rates of sediment accumulation, considering that 390 cm of sediments were deposited since 550 CE. Studies (e.g Jòhansen, 1985) that have employed macrofossils as their dating targets have in some occasions displayed inconsistent results. However, radiocarbon dates does not always represent the age of the material itself, and there are several sources for errors, including presence of nuclear bombing, uptake of carbon in reservoir, and contamination by incorporation old or younger carbon residues. The radiocarbon analyses reveal that one radiocarbon date 940 cal. yr. BP (Poz-110010) is inconsistent with the position in the composite sediment record and rejected by the age-depth model (Figure 14). The results (Figure 18) show that the date is located by a rapid increase of organic material at 79.8 cm depth in LEP-01-15 (associated with section 4.4.1

unit C). Hence, the inverted date is likely caused by contamination of extensive in-wash of older terrestrial material or carbon from local bedrock. Note, that samples with even small amounts of contamination can produce major errors in radiocarbon dates. The error will increase with the age of the carbon being incorporated. For instance, adding 1% old carbon to a modern sample will increase the age by several hundred years depending on how old the incorporated carbon is (Walker, 2005, p. 24-25).

It is essential that a reliable age-depth model is constructed when reconstructing climate variability. Some of the crucial restrictions are:

1. Dating samples of great age control
2. The sedimentation is increasing monotonically with depth
3. Should not have hiatus or disturbed sections

The results from Table 2 indicate a clear agreement between the dated samples at 104.5 cm, 150 cm, and 202.5 cm depth in LEP-01-15, which could be interpreted as a possible instantaneous deposit. However, the model computed age depth curve invalidates the sample at 104.5 cm (Figure 15). The age-depth model and the constructed sediment accumulation history must be treated with caution, due to problems of securing accurate radiocarbon dating.

Element counts and element ratios (i.e. Ti (titanium), Ca (calcium), K (potassium), Mn (manganese), Fe (iron) and (incoh/coh)) presented in Figures 22 and 23 are widely used as environmental proxies for lake sediment records (Croudace & Rothwell, 2015). Note that all raw XRF-scanning results are shown as 35 point running average profiles, since it is the relative changes, rather than the absolute concentration, that are of interest on a environmental context. The geochemial elements Ti, K and Ca display similar variability to DBD and are interpreted to reflect the amount of inorganic input from erosion and weathering of bedrock and soils within the lake catchment (Croudace & Rothwell, 2015; De Wet, 2017; Kylander, Ampel, Wohlfarth, & Veres, 2011; Olsen et al., 2010).

Thus, the DBD is indicative of the overall sediment compactness. The down-core concentration of Ti and K counts can also be controlled by particle sizes and effected by the clay mineral assemblages (Kylander et al., 2011). Specific element can also provide valuable insights in past events, such as K counts can show the presence of tephra particles (De Wet, 2017). Although, K counts in Figure 23 display similar variability with Ti and Ca counts. The redox sensitive elements Fe and Mn have a moderate to strong relationship, which suggest that they are potentially indicative for weathering conditions in the lake, detrital input or changes in sediment source. The (incoh/coh) ratio has previous (e.g. (Chawchai, Kylander, Chabangborn, Lowemark, & Wohlfarth, 2016)) been applied as a proxy for the abundance of organic-rich sediments or reflecting changes in density and water content. The incoh/coh scattering ratio is a bulk ratio and relates to the average atomic number of the sample. Materials with low atomic numbers (e.g. organic rich sediments) will generate high incoherent and low coherent scattering values. Thus, the (incoh/coh) ratio is affected by all components of the sediment. The XRF scanning results are semi-quantitative measurements (Croudace et al., 2006). Changes in sediment density, water content, organic matter, grain size, mineralogy or surface roughness can cause absorption or scattering. For instance, samples that are heterogeneous (low densities and high water content) can be problematic as such sediments can absorb x-ray radiation. This affects the XRF analysis in that lower fluorescence energies are emitted from the core, causing weaker measured signals particularly for lighter elements (Chawchai et al., 2016). Therefore, the XRF analysis must be compared with other proxies to support the elemental interpretations.

The magnetic susceptibility (MS) gathers essential information about the magnetic properties of the composite sediment record. It co-varies with the geochemical elements Ti, Ca and K, which suggest that the validity of the proxies quantifies the amount of inorganic delivery to Leynavatn. Note, that the MS analysis provide relative magnetic measurements, because the results can fluctuate if the point sensor is not in contact with the core surface.

The LOI can show relative quantity of organic material in sediment cores (Nesje et

al., 2000). The comparison between the incoh/coh ratio and loss-on-ignition (LOI) profile show similar patterns, which support the assumption that (incoh/coh) ratio can be applied as a proxy for organic content (Figure 22). Changes in LOI can trace various sediment delivery, where low LOI percentages indicate inorganic-rich and higher percentages more organic-rich layers. To some extent, the incoh/coh ratio and the LOI correlate inversely with the magnetic susceptibility and the geochemical elements Ti, K, Ca.

The CT-scan and the radiographic images determine continuous laminations in the Leynavatn record and also verifies that the sediments in the record were not deposited instantaneous. In addition, the x-ray CT results reveal distinct particles in matrix-supported layers. The transport and depositional environment for such particles are challenging to interpret, but could possibly represent episodes of lake freezing, tephra particles, or periods with enhanced weathering.

Moreover, the sediment record from Leynavatn can display the possibility of a catastrophic ash fallout event (e.g. hekla-1 or öræfajökull). Given that the Faroes are a potential area for tracing the most widely dispersed volcanic events from the last millennium (Hannon & Bradshaw, 2000). However, no distinct tephra horizons were visually found in the LEP-01-15 and LED-01-15. Although, it is possible that both macro- and cryptotephra layers can still manifest itself as raised clastic material input and lowered input of other major components (e.g. organic material, biogenic silica).

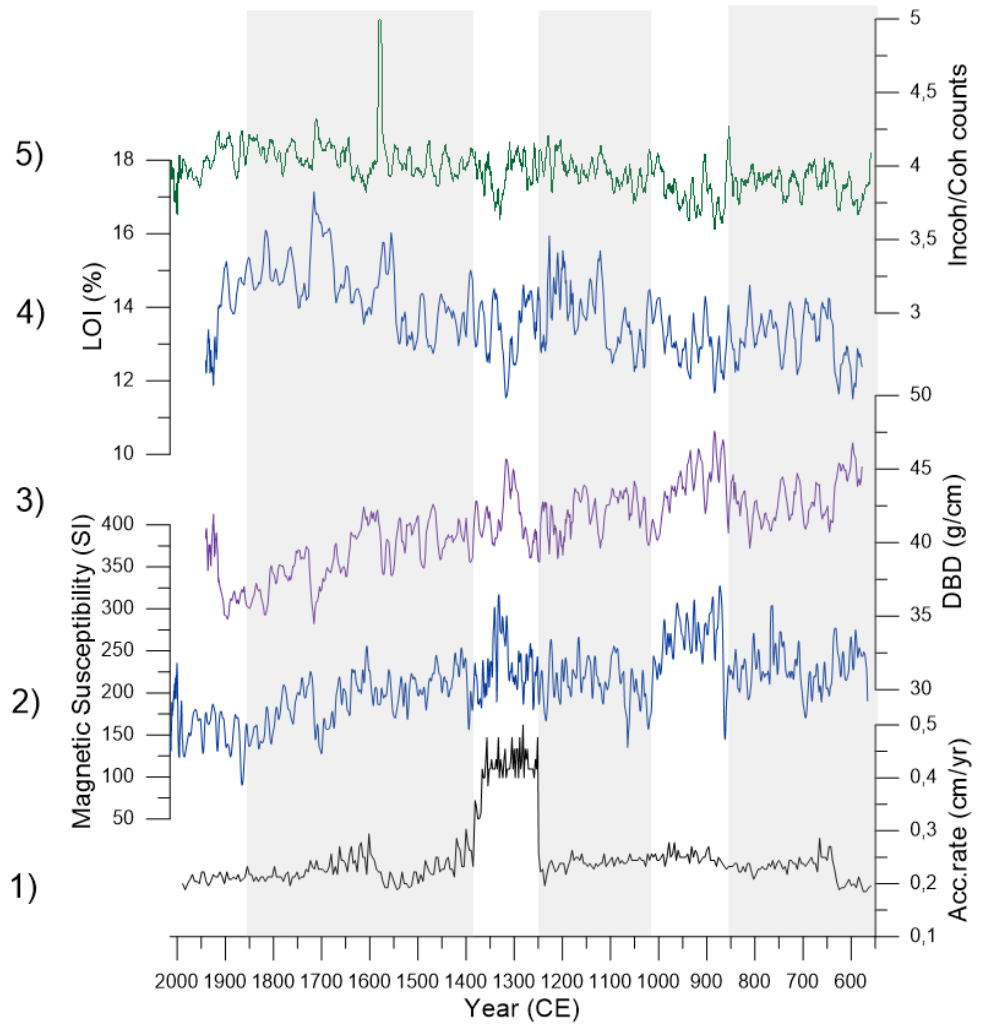

Figure 22: *Summary diagram of the composite Leynavatn record: 1) Sediment accumulation rate; 2) Magnetic susceptibility; 3) Dry bulk density; 4) Loss-on-ignition; 5) Ratio between incoherent and coherent scattering. The environmental changes are outlined with white or grey background color. Note, that the magnetic susceptibility co-varies with the dry bulk density and inversely corresponds with the loss-on-ignition and incoherent/coherent scattering ratio. The sediment accumulation show an abrupt rise at 1250-1375 CE.*

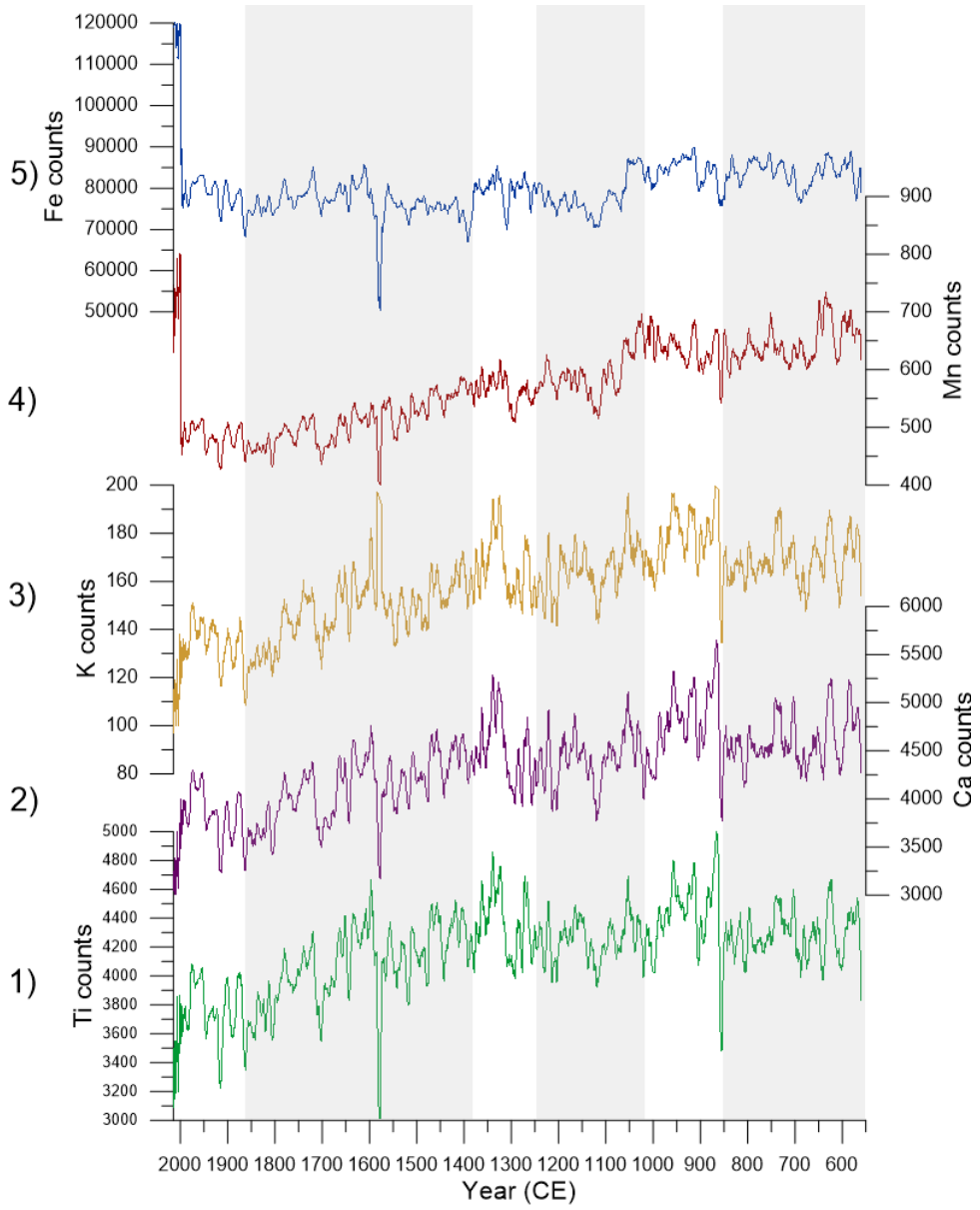

Figure 23: *Selected elemental counts from Itrax XRF core scanning for composite Leynavatn record: 1) Titanium; 2) Calsium; 3) Potassium; 4) Manganese; 5) Iron. The environmental changes are outlined with white or grey background color. Note, that the geochemical elements Ti, Ca, and K are comparable, despite the Mn and Fe which are less corresponding.*

5.3 Climate implications

To investigate climatic induced changes and the sediment delivery to Leynavatn, the physical properties of Leynavatn sediment record is compared with representative records of North Atlantic Oscillation (NAO) and warm season Sea Surface Temperatures (SST) covering the last two millennium (Figure 25). The SST and NAO must be considered when evaluating the climate development at Leynavatn, Faroe Islands because it effects the weather events and long term landscape development (Adderley & Simpson, 2005).

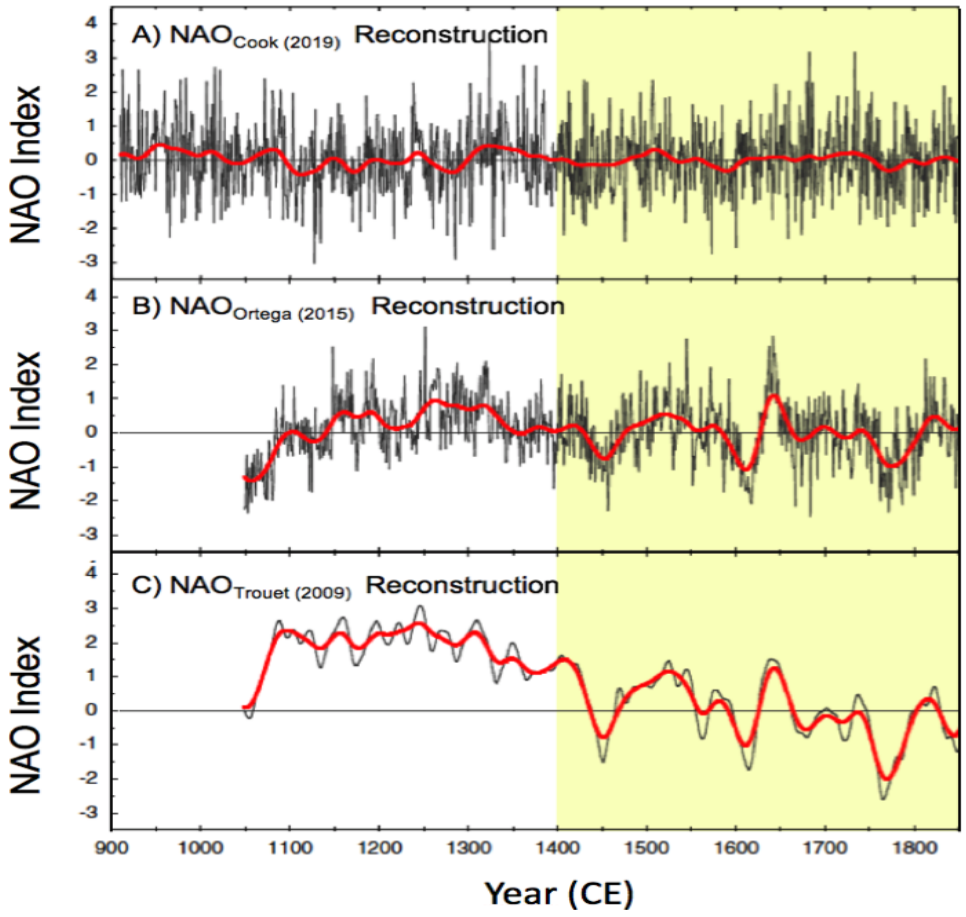

Figure 24: *Comparing tree different NAO reconstructions extending back to the medieval period. A) NAO_{Cook}, B) NAO_{Ortega}, C) NAO_{Trouet}. Each reconstruction (black profile line) has been smoothed with a 50 yr filter (red profile line) which highlight the NAO variability. The yellow background shading represents the Little Ice Age. Note, the transition from MWP to LIA at 1400 CE. Modified from (Cook et al., 2019).*

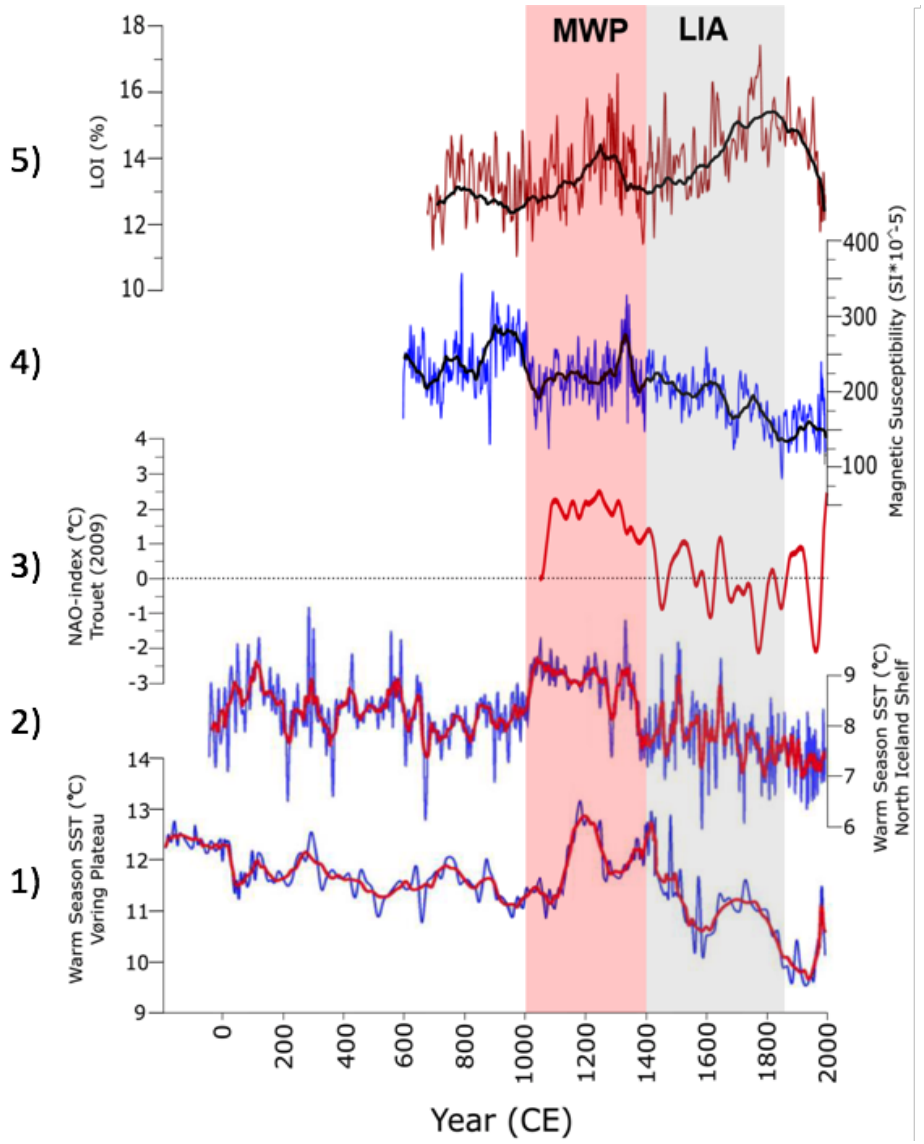

Figure 25: *Comparing climate records from the North Atlantic region: 1) Vøringen Plateau SST (red line 5-point smooth); 2) North Iceland Shelf SST (red line 5-point smooth); 3) NAO reconstruction by Trouet (2009) (red line 50 yr smooth); 4) Composite Leynavatn magnetic susceptibility record from LEP-01-15 and LED-01-15 (black line 73-point smooth); 5) Composite Leynavatn loss-on-ignition record from LEP-01-15 and LED-01-15 (black line 73-point smooth). MWP (red) and LIA (grey) interval shown by vertical background shading. Note, during the transition from MWP to LIA the LOI profile increases and the magnetic susceptibility decreases persistently with the NAO ans SST records.*

5.3.1 550-850 CE

At the base of Leynavatn sediment record, the magnetic susceptibility (MS) show shifting inorganic delivery, which has a decreasing trend until 700 CE. The Loss-on-Ignition (LOI) reflecting organic delivery correlate inversely with the inorganic input. SST reconstructions from the North Iceland Shelf (Sicre et al., 2008) show a small decreasing temperature trend, despite minor fluctuations representing ocean variability. This reflects changes in organic and inorganic material delivery to Leynavatn during a slightly cooler time period.

5.3.2 850-1000 CE

The arrival of extensive human settlement can be considered as an explanation for the increased MS in the Leynavatn sediment record shown in Figure 25. Section 2.4 suggest that inflation of humans, their agricultural system and livestock must have a contributing effect on the landscape. The livestock (especially sheep) will break up the vegetation that binds the topsoil together, partly by eating down to the roots, tramping holes on the surface and walking on unstable slopes (Adderley & Simpson, 2005; Arge, 2014). The result of overgrazing, trampling and deforestation will create new ways for wind and water to flow, thus accelerating the erosion rate in the catchment area and depositing more inorganic material to the lake basin. The SST records from the Vøringen Plateau show cooler ocean temperatures, while the SST record from north Iceland Shelf is persistent at around 8 °C. The SST reconstruction from Vøringen plateau (eastern Norwegian sea) is based on geochemical and faunal analysis of planktic foraminifers (Andersson et al., 2003). However, the north Iceland shelf display SST reconstructions estimated by alkenone biomarkers (Sicre et al., 2008). The two SST records from the North Atlantic does not always coincide with another, still they show similar temporal and spatial patterns related to the North Atlantic thermohaline circulation. Cook (2009) NAO reconstruction NAO_{Cook} display a small amplitude positive NAO phase. NAO_{Cook} is based on annually resolved moisture sensitive tree-ring records (Cook et al., 2019).

5.3.3 1000-1250 CE

The Leynavatn proxies show increased organic delivery, whereas the inorganic delivery is sustained with smaller variable amplitudes. Both the SST records exhibit prolonged warm temperatures from 1000-1450 CE and the north Icelands shelf display an increase of 1-1.5 °C at 1150 CE. Trouet (2009) NAO reconstructions (NAO_{Trouet}) show a predominantly positive NAO phase at 1000-1450 CE. This record is generated by tree-rings from Morocco and speleothems from Scotland, which are not annually resolved (Trouet et al., 2009). Furthermore, Ortega (2015) NAO reconstruction (NAO_{Ortega}) differs from NAO_{Trouet} and does not show a persistent NAO phase. The NAO_{Ortega} reveals positive phases during 1150-1200 CE. Thus, NAO_{Ortega} is based on a large set of annually resolved proxy records distributed around the North Atlantic (Ortega et al., 2015). The NAO_{Ortega} and NAO_{Trouet} suggest a positive NAO phase during the beginning of the second millennium. A positive NAO and increase SSTs can relate to moist and warm conditions where more frequent storms and extreme weather events effect the Faroes. This distinct time interval can display the onset of the medieval warm period (MWP).

5.3.4 1250-1375 CE

A prolonged period where the landscape became unstable may have existed at Leynavatn 1250-1375 CE. The age model show three consistent radiocarbon dates, while Figure 25 reveal elevated MS and decreasing LOI (section 4.4.1 Unit D). These trends can be interpreted to show a substantial input of allochthonous material. Also, high sedimentation rate (0.45 cm/yr), compared to normal sediment production in Leynavatn is evident. The high sedimentation rate may act as a indicator for episodic events such as floods, extreme weather and avalanches. However, the x-ray CT analysis (Figure 21b) show laminated sediments. The laminations indicate that the high sedimentation is not an instantaneous deposit, but can appear as decadal or annual events where enhanced weathering and soil instability produced distinct sediment layers. During the persistent warmer SSTs, a brief episode of colder SSTs at 1300-1350 CE is shown in both SST records. All the

NAO records NAO_{Trouet}, AO_{Ortega} and NAO_{Cook} display positive NAO phases of different amplitudes and strengthen the interpretation of a medieval warm period. In fact, McGowan (2008) supports the idea that exceptionally high rates of sediment accumulation, increase LOI and MS can reflect a period of elevated soil erosion due to regional climate deterioration.

5.3.5 1375-1850 CE

The MS show a decreasing trend in inorganic delivery to the lake (Figures 22 and 23). However, the LOI reflects conditions where organic delivery increased. The LOI record deviates from the mentioned climate records, because it does not associate with continually cooler conditions. The LOI can be explained by high amounts of detrital surface run-off, or that the catchment became more productive during the period. This may also explain the inverted radiocarbon date found in LEP-01-15 at 79.8 cm depth. In addition, layers with high particle concentration are found at 54 cm and 64 cm depth in LEP-01-15 (Figure 20a). Andresen (2006) considers such evidence to prove conditions where the lake had ice cover. The concept of Andresen‘s assumption is based on the transport of grains larger than 225 µm to the center of a flat bottomed lake, which has to be mediated by lake freezing. The SSTs at Vøringen plateau and N. Atlantic shelf cools persistently for several centuries (T. M. Cronin et al., 2010). Such temperature cooling is also visible in the NAO_{Trouet} and NAO_{Ortega} during 1450, 1600 and 1750 CE. The NAO_{Trouet} and NAO_{Ortega} correspond with one another, considering that the amplitude of NAO_{Ortega} is smaller than NAO_{Trouet}. The northern hemisphere temperature cooling can refer to the Little Ice Age (LIA) reflecting conditions where high-frequency of cold summers and cold winters appeared from 1400-1850 CE (T. M. Cronin et al., 2010; Amorosi et al., 1997). The LIA is usually described by the glacier advances recorded in all parts of the globe. Although, it is composed of several periods when glacier extent were larger (Wanner et al., 2008). Multiple mechanisms is suggested as factors influencing the LIA, where the most reliable explanation is a combination of volcanic, orbital and solar forcing. A setting were high-frequency volcanic eruptions but less solar activity could potentially initiate

the LIA cooling.

5.3.6 1850 CE to present day

The period from 1850 CE to the present day is interpreted as the transition from cooler conditions representing the LIA towards 1900 CE warming conditions (Amorosi et al., 1997). The Leynavatn sediment proxies illustrate decreasing organic influx, despite variable inorganic delivery. The NAO_{Trouet} is abruptly shifting towards a positive NAO phase (Figure 25) and SSTs representative for the north Atlantic region is slightly increasing, especially the SST record from the Vøring plateau SST. Temperatures are increasing and a strong positive NAO reflect a warm phase were anthropogenic signals can have a significant impact.

The results from the Leynavatn sediment record together with the studies mentioned above shed light on patterns of climate variability since the 550 CE. It is difficult to accurately determine the timing and nature of the changes detected in Leynavatn sediment record. However, it is evident that the MWP and LIA differ significantly in terms of physical and geochemical sediment properties. For instance, proxies derived from sediments recovered at Leynavatn show multidecadal scale shifts in inorganic and organic influx as a result of catchment processes. The firm chronology suggest that late Holocene climate fluctuations causes extreme weather conditions, which would have a great influence on the landscape and the sediment source to Leynavatn. The Leynavatn record covers the time before and during the first settlement. Hence, the unstable landscape could also be greatly influenced by human impact. Whether the change in Leynavatn sediment record is caused by natural or anthropogenic disturbances is difficult to unravel.

6 Summary and Conclusions

- The presented terrain model and geomorphological map in section 4.1 gives an overview of the processes that potentially effects the sediment delivery to Leynavatn. The surrounding landscape host several sediment deposits and erosion features, including colluvial aprons, rockfall, debris flows and fluvial deposits. This indicates that the terrestrial geomorphology response to changes relating to anthropogenic disturbance and climate instability.

- Extreme weather events, heavy rainfall, strong winds and grazing sheep will cause extensive erosion of the landscape and high sediment influx to Leynavatn. As a consequence, the sediment cores LEP-01-15 and LED-15-1 only covers the time period 550-2015 CE.

- Leynavatn sediment proxies show that allochthonous influx were sufficient to cause substantial changes in the geochemical and physical properties. The interpretation in section 5.2 reveal that magnetic susceptibility reflect the amount of inorganic delivery, while the loss-on-ignition display variation in amount of organic material in the composite sediment record.

- Decadal shifts following the MWP and LIA is evident when integrating the findings in a regional paleoclimatic context. During 1250-1375 CE increased sediment accumulation, high magnetic susceptibility, laminated sediments and consistent radiocarbon dates in the Bayesian age-depth model, suggest a warming phase referring to the MWP. After the 1400 CE the proxies show persistently decreasing magnetic susceptibility, increased loss-on-ignition and distinct sediment layers with high particle concentration. These changes can be associated with the LIA cooling phase.

6.1 Further work

There are several errors to this study, and further research of other lakes in the Faroes will need to take place to strengthen the theories of late Holocene climate events. In addition, there are more robust reconstructions that can be obtained through multi-proxy analysis, such as biological proxies and aquatic systems. These can be useful since they respond directly to climate variability. In addition, studying cryptotephras and tephra deposits within soil sections is an important complement to the geological chronology, because it can improve age models, reduce age uncertainties and test other dating techniques.

References

Adderley, W. P., & Simpson, I. A. (2005). Early norse home-field productivity in the faroe islands. *Human Ecology*, *33*(5), 711–737.

Aken, H. M. v. (2007). *The oceanic thermohaline circulation : an introduction* (Vol. 39). New York: Springer.

Amorosi, T., Buckland, P., Dugmore, A., Ingimundarson, J. H., & McGovern, T. H. (1997). Raiding the landscape: Human impact in the scandinavian north atlantic. *Human Ecology*, *25*, 491–518.

Andersson, C., Risebrobakken, B., Jansen, E., & Dahl, S. O. (2003). Late holocene surface ocean conditions of the norwegian sea (vøring plateau). *Paleoceanography*, *18*(2), 22-1–13.

Andresen, C. S., Björck, S., Rundgren, M., Conley, D. J., & Jessen, C. A. (2006). Rapid holocene climate changes in the north atlantic: evidence from lake sediments from the faroe islands. *Boreas*, *35*, 23–34.

Arge, S. V. (1991). The landnám in the faroes. *Arctic Anthropology*, *28*(2), 101–120.

Arge, S. V. (2014). Viking faroes: Settlement, paleoeconomy, and chronology. *Journal of the North Atlantic*, *7*, 1–17.

Arge, S. V., Sveinbjarnardóttir, G., Edwards, K. J., & Buckland, P. C. (2005). Viking and medieval settlement in the faroes: People, place and environment. *Human Ecology*, *33*(5), 597–620.

Blaauw, M., & Christen, J. A. (2011). Flexible paleoclimate age-depth models using an autoregressive gamma process. *Bayesian Analysis*, *6*(3), 457–474.

Blikra, L. H. (1990). Geological mapping of rapid mass movement deposits as an aid to land-use planning. *Engineering Geology*, *29*, 365–376.

Blikra, L. H., & Nemec, W. (1998). Postglacial colluvium in western norway: depositional processes, facies and palaeoclimatic record. *Sedimentology*, *45*(5), 909–959.

Boyle, J. F. (1995). A simple closure mechanism for a compact, large-diameter, gravity corer. *Journal of Paleolimnology*, *13*, 85–87.

Bradley, R. S. (2014). *Paleoclimatology: reconstructing climates of the quaternary* (3rd ed. ed.). Amsterdam: Academic Press.

Chawchai, S., Kylander, M. E., Chabangborn, A., Lowemark, L., & Wohlfarth, B. (2016). Testing commonly used x-ray fluorescence core scanning-based proxies for organic-rich lake sediments and peat. *Boreas*, *45*, 180–189.

Church, M. J., Arge, S. V., Brewington, S., McGovern, T. H., Woollett, J. M., Perdikaris, S., Lawson, I. T., Cook, G. T., Amundsen, C., Harrison, R., Krivogorskaya, Y., & Dunbar, E. (2005). Puffins, pigs, cod and barley: Palaeoeconomy at undir junkarinsfløtti, sandoy, faroe islands. *Environmental Archaeology*, *10*, 179–197.

Church, M. J., Arge, S. V., Edwards, K. J., Ascough, P. L., Bond, J. M., Cook, G. T., Dockrill, S. J., Dugmore, A. J., McGovern, T. H., Nesbitt, C., & Simpson, I. A. (2013). The vikings were not the first colonizers of the faroe islands. *Quaternary Science Reviews*, *77*, 228–232.

Cnudde, V., & Boone, M. N. (2013). High-resolution x-ray computed tomography in geosciences: a review of the current technology and applications. *Earth Science Reviews*, *123*, 1–17.

Cook, E. R., Kushnir, Y., Smerdon, J. E., Williams, A. P., Anchukaitis, K. J., & Wahl, E. R. (2019). A euro-mediterranean tree-ring reconstruction of the winter nao index since 910 c.e. *Clim Dyn*, 1–14.

Cronin, T. (2009). *Paleoclimates : Understanding climate change past and present.* New York: Columbia University Press.

Cronin, T. M., Hayo, K., Thunell, R. C., Dwyer, G. S., Saenger, C., & Willard, D. A. (2010). The medieval climate anomaly and little ice age in chesapeake bay and the north atlantic ocean. *Palaeogeography, Palaeoclimatology, Palaeoecology*, *297*(2), 299–310.

Croudace, I. W., Rindby, A., & Rothwell, R. G. (2006). Itrax; description and evaluation of a new multi-function x-ray core scanner. *Geological Society, London, Special Publications*, *267*, 51–63.

Croudace, I. W., & Rothwell, R. G. (2015). *Micro-xrf studies of sediment cores: Applica-*

tions of a non-destructive tool for the environmental sciences (Vol. 17). Dordrecht: Springer Netherlands.

Dean, W. E. (1974). Determination of carbonate and organic matter in calcareous sediments and sedimentary rocks by loss on ignition; comparison with other methods. *Journal of Sedimentary Petrology*, *44*(1), 242–248.

De Wet, G. A. (2017). *Arctic and north atlantic paleo-environmental reconstructions from lake sediments.* Amherst, Massachusetts.

Dugmore, A. J., Church, M. J., Buckland, P. C., Edwards, K. J., Lawson, I., McGovern, T. H., Panagiotakopulu, E., Simpson, I. A., Skidmore, P., & Sveinbjarnardottir, G. (2005). The norse landnám on the north atlantic islands: an environmental impact assessment. *Polar Record*, *41*, 21–37.

Edwards, K. J., Borthwick, D., Cook, G., Dugmore, A. J., Mairs, K. A., Church, M. J., Simpson, I. A., & Adderley, W. P. (2005). A hypothesis-based approach to landscape change in suðuroy, faroe islands. *Human Ecology*, *33*(5), 621–650.

Gathorne-Hardy, F. J., Lawson, I. T., Church, M. J., Brooks, S. J., Buckland, P. C., & Edwards, K. J. (2007). The chironomidae of gróthúsvatn, sandoy, faroe islands: climatic and lake-phosphorus reconstructions, and the impact of human settlement. *The Holocene*, *17*(8), 1259–1264.

Gunn, D. E., & Best, A. I. (1998). A new automated nondestructive system for high resolution multi-sensor core logging of open sediment cores. *Geo-Marine Letters*, *18*, 70–77.

Guttesen, R. (1996). *Atlas of danmark: The faeroe islands topography atlas* (Vol. 5). Det Kongelige Danske Geografiske Selskap.

Hannon, G. E., & Bradshaw, R. H. (2000). Impacts and timing of the first human settlement on vegetation of the faroe islands. *Quaternary Research*, *54*, 404–413.

Hannon, G. E., Bradshaw, R. H. W., Bradshaw, E. G., Snowball, I., & Wastegard, S. (2005). Climate change and human settlement as drivers of late-holocene vegetational change in the faroe islands. *Holocene*, *15*(5), 639–647.

Hannon, G. E., Hermanns-Auðardóttir, M., & Wastegård, S. (1998). Human impact at

tjørnuvík in the faroe island. *Fróðskaparrit*, *46*, 215–228.

Hannon, G. E., Wastegård, S., Bradshaw, E. G., & Bradshaw, R. H. W. (2001). Human impact and landscape degradation on the faroe islands. *Biology and Environment: Proceedings of the Royal Irish Acadamy*, *101B*(1-2), 129–139.

Humlum, O. (1998). Rock glaciers on the faeroe islands, the north atlantic. *Journal of Quaternary Science*, *13*(4), 293–307.

Humlum, O., & Christiansen, H. H. (1998). *Late holocene climatic forcing of geomorphic activity in the faroe islands* (Vol. 46). fróðskaparrit.

Humlum, O., Christiansen, H. H., Svensson, H., & Mortensen, L. E. (1996). Moraine systems in the faroe islands: Glaciological and climatological implications. *Danish Journal of Geography*, *96*, 21–31.

Jóhansen, J. (1985). *Studies in the vegetational history of the faroe and shetland islands* (Vol. 11). Torshavn.

Kuijpers, A., Troelstra, S. R., Wisse, M., Heier Nielsen, S., & van Weering, T. C. E. (1998). Norwegian sea overflow variability and ne atlantic surface hydrography during the past 150,000 years. *Marine Geology*, *152*, 75–99.

Kylander, M. E., Ampel, L., Wohlfarth, B., & Veres, D. (2011). High-resolution x-ray fluorescence core scanning analysis of les echets (france) sedimentary sequence; new insights from chemical proxies. *Journal of Quaternary Science*, *26*(1), 109–117.

Landkildehus, F., Jeppesen, E., Jensen, J. P., & Dali, S. (2002). General description of five faroese lakes. *Ann. Soc. Scient. Færoensis Suppl*, *36*, 28–33.

Larsen, L. M., Waagstein, R., Pedersen, A. K., & Storey, M. (1999). Trans-atlantic correlation of the palaeogene volcanic successions in the faeroe islands and east greenland. *Journal Of The Geological Society*, *156*, 1081–1095.

Lawson, I. T., Church, M. J., McGovern, T. H., Arge, S. V., Woollet, J., Edwards, K. J., Gathorne-Hardy, F. J., Dugmore, A. J., Cook, G., Mairs, K. A., Thomson, A. M., & Sveinbjarnardótti, G. (2005). Historical ecology on sandoy, faroe islands: Palaeoenvironmental and archaeological perspectives. *Human Ecology*, *33*(5), 651–684.

Malmquist, H. J., Ingimarsson, F., Jóhannsdóttir, E. E., Òlafsson, S., J, & Gíslason, G. M. (2002). Zoobenthos in the littoral and profundal zones of four faroese lakes. *Ann. Soc. Scient. Færoensis Suppl*, *36*, 79–93.

Mcgowan, S., Grauert, M., & Anderson, N. J. (2008). A late holocene record of landscape degradation from heygsvatn, the faroe islands. *Palaeogeography, Palaeoclimatology, Palaeoecology*, *264*(1), 11–24.

Munsell, A. H., & Color, M. (2000). *Munsell soil color charts* (2000th ed.). Munsell Color.

Nesje, A. (1992). A piston corer for lacustrine and marine sediments. *Arctic and Alpine Research*, *24*(3), 257–259.

Nesje, A., Dahl, S. O., Andersson, C., & Matthews, J. A. (2000). The lacustrine sedimentary sequence in sygneskardvatnet, western norway: a continuous, high-resolution record of the jostedalsbreen ice cap during the holocene. *Quaternary Science Reviews*, *19*, 1047–1065.

Nielsen, T., Rasmussen, T. L., Ceramicola, S., & Kuijpers, A. (2007). Quaternary sedimentation, margin architecture and ocean circulation variability around the faroe islands, north atlantic. *Quaternary Science Reviews*, *26*(7), 1016–1036.

Olsen, J., Björck, S., Leng, M. J., Gudmundsdóttir, E. R., Odgaard, B. V., Lutz, C. M., Kendrick, C. P., Andersen, T. J., & Seidenkrantz, M.-S. (2010). Lacustrine evidence of holocene environmental change from three faroese lakes: a multiproxy xrf and stable isotope study. *Quaternary Science Reviews*, *29*, 2764–2780.

Ortega, P., Lehner, F., Swingedouw, D., Masson-Delmotte, V., C, R. C., Casado, M., & Yiou, P. (2015). A model-tested north atlantic oscillation reconstruction for the past millennium. *Nature*, *523*, 71–74.

Passey, S. R., & Bell, B. R. (2007). Morphologies and emplacement mechanisms of the lava flows of the faroe islands basalt group, faroe islands, ne atlantic ocean. *Bull Volcanol*, *70*, 139–156.

Pinto, J. G., & Raible, C. C. (2012). Past and recent changes in the north atlantic oscillation. *WIREs Climate Change*, *3*, 79–90.

Rasmussen, T. L., & Thomsen, E. (2010). Holocene temperature and salinity variability of the atlantic water inflow to the nordic seas. *The Holocene*, *20*(8), 1223–1234.

Sicre, M. A., Jacob, J., Ezat, U., Rousse, S., Kissel, C., Yiou, P., Eiríksson, J., Knudsen, K. L., Jansen, E., & Turon, J. L. (2008). Decadal variability of sea surface temperatures off north iceland over the last 2000 years. *Earth and Planetary Science Letters*, *268*, 137–142.

Trouet, V., Esper, J., Graham, N. E., Baker, A., Scourse, J. D., & Frank, D. C. (2009). Persistent positive north atlantic oscillation mode dominated the medieval climate anomaly.). *Science*, *324*, 78–80.

Visbeck, M. H., Hurrell, J. W., Polvani, L., & Cullen, H. M. (2001). The north atlantic oscillation: Past, present, and future. *National Acad Sciences*, *98*(23).

Walker, M. J. C. (2005). *Quaternary dating methods*. Chichester: John Wiley & Sons Ltd.

Wanner, H., Beer, J., Bütikofer, J., Crowley, T. J., Cubasch, U., Flückiger, J., Goosse, H., Grosjean, M., Joos, F., Kaplan, J. O., Küttel, M., Müller, S. A., Prentice, I. C., Solomina, O., Stocker, T. F., Tarasov, P., Wagner, M., & Widmann, M. (2008). Mid- to late holocene climate change: an overview. *Quaternary Science Reviews*, *27*, 1791–1828.

Wastegård, S., Björck, S., Grauert, M., & Hannon, G. E. (2001). The mjáuvøtn tephra and other holocene tephra horizons from the faroe islands: a link between the icelandic source region, the nordic seas, and the european continent. *The Holocene*, *11*(1), 101–109.

Online

Blaauw, M., & Christen, J. A. (2013). Bacon manual-v.2.2. Retrieved 2019-02-18, from http://www.chrono.qub.ac.uk/blaauw/bacon.html

Cappelen, J & Laursen, E. V. (1998). The Climate of The Faroe Islands - with Climatological Standard Normals, 1961-1990. DMI Technical Report 98-14. Copenhagen. Retrieved 2019-05-28, from

https://www.dmi.dk/fileadmin/user_upload/Rapporter/TR/1998/tr98-14.pdf

Porter, C., Morin, P., Howat, I., Noh, M.-J., Bates, B., Peterman, K., Keesey, S., Schlenk, M., Gardiner, J., Tomko, K., Willis, M., Kelleher, C., Cloutier, M., Husby, E., Foga, S., Nakamura, H., Platson, M., Wethington, J., Michael, Williamson, C., Bauer, G., Enos, J., Arnold, G., Kramer, W., Becker, P., Doshi, A., D'Souza, C., Cummens, P., Laurier, F., & Bojesen, M. (2018). ArcticDEM. Harvard Dataverse. Retrieved 2019-03-01, from https://doi.org/10.7910/DVN/OHHUKH